Dedication

To my beloved parents I love you so much

You always be in my heart

To my sisters

To my friends

To my close friends

Thanks a bunch

Anis

To my beloved family and friends, your unwavering support has fueled my academic journey and personal growth. To myself, for the determination, discipline, and passion that drove my thirst for knowledge. This work embodies my development and resilience, reminding me of my ability to overcome challenges and make meaningful contributions to my field. May this work advance knowledge and unlock future opportunities. I dedicate it to all who played a vital role in my journey. Your encouragement and belief in me have been truly priceless. Thank you!

Oussama

Acknowledgement

In the name of ALLAH, the Most Gracious and the Most Merciful.

Thanks to ALLAH, for the strengths and guidance in completing this work. It is our belief in him that helped us persevere at times when it seemed impossible to go on.

We would like to express our deep-felt gratitude to our supervisor ***Dr. Abdelkarim AMMAR*** *for his wisdom, guidance and support.*

We would like to thank our colleague ***Hamza BELMADANI*** *for his help.*

We take this opportunity to record our sincere thanks to all IGEE teachers.

Abstract

This work presents a comprehensive investigation of a single-stage battery-less stand-alone solar water pumping system, utilizing an induction motor for pump operation. A double function voltage source inverter (VSI) controlled by a switching table based on direct torque control (DTC), and employing Maximum Power Point Tracking (MPPT) techniques to optimize system performance. The primary objective is to evaluate the system's behavior and efficiency under normal and shaded conditions by implementing various MPPT algorithms, including Perturb and Observe (P&O), Particle Swarm Optimization (PSO), and Grey Wolf Optimization (GWO). The research begins with an in-depth analysis of the system components, including the solar panels, inverter, induction motor, and MPPT algorithms. Theoretical aspects of the induction motor, VSI, DTC, and MPPT techniques are studied to establish a solid understanding of their interactions within the solar water pumping system. A test setup is implemented, simulating real-world scenarios to evaluate the system's response and efficiency. Data is collected, and comparative analysis are performed to determine the effectiveness of each MPPT algorithm in terms of tracking the maximum power point, optimizing power output under partial shading condition.

Keywords:

Solar Water Pumping System (SWPS), Partial shading, Induction Motor (IM), Voltage Source Inverter (VSI), Direct Torque Control (DTC), Maximum Power Point Tracking (MPPT), Perturb and Observe (P&O), Particle Swarm Optimization (PSO), Grey Wolf Optimization (GWO).

Table of contents

List of Tables

List of figures

List of abbreviation

P: power [w].

I: current [A].

V: voltage [V].

PV: photovoltaic.

MPPT: maximum power point tracking.

P&O: perturb and observe.

DTC: direct torque control.

SWP: solar water pumping.

SWPS: solar water pumping system.

WPS: Water pumping system.

BLDC: brushless Dc motor.

IM: induction motor.

VSI: voltage source inverter.

D: diode.

SPV: solar photovoltaic.

VSC: voltage source converter.

CSI: current source inverter.

THD: total harmonic distortion.

PWM: pulse width modulation.

KVL: krichoff's voltage law.

KCL: krichoff's current law.

STC: standard test conditions [25°C, 1sun].

MOSFET: Metal Oxide Semiconductor Field Effect Transistor.

IGBT: Insulated Gate Bipolar Transistor.

GWO: grey wolf optimization.

PSO: particle swarm optimization.

MPP: maximum power point.

LP: local peak.

GP: global peak.

GAs: Genetic algrotihms

List of Symbols

I_{ph}: The Photocurrent, is the current produced by the incident light and function of irradiation level and junction temperature in Amps.

I_D: The diode current modeled by the equation for a Shockley diode in Amps.

I_o: The saturated reverse current or leakage current in Amps.

q: Electron charge (1.602 × 10-19 C).

K: Boltzmann constant (1.38 x 10 -23 J/°K).

V: Cell output voltage, (V).

T_o: Cell operating temperature, °K.

A: The diode ideality factor.

$R_{s,\,cell}$: Series resistance of the cell, Ohm.

$R_{sh,cell}$: Shunt resistance of the cell, Ohm.

$R_{sh,module}$: Total shunt resistance in the photovoltaic module, Ohm.

$R_{s,module}$: Total series resistance in the photovoltaic module, Ohm.

V_t: Thermal voltage, V.

N_s: Number of series cells.

N_p: Number of cells branches in parallel.

$I_{sc,module}$: Total short circuit current of the photovoltaic module, A.

$V_{oc,module}$: Total open circuit voltage of the photovoltaic module, V.

$I_{sc,cell}$: Short circuit current of one photovoltaic cell.

$V_{oc,cell}$: Open circuit voltage of one photovoltaic cell.

V_{array}: the terminals voltage of the array.

I_{array}: the output current of the pv array.

R_s: is the stator resistance.

L_s: is the stator inductance.

V_r: is the rotor voltage.

I_r: is the rotor current.

R_r: is the rotor resistance.

L_r: is the rotor inductance.

ω_m: is the mechanical angular velocity.

ω_r: is the electrical angular velocity.

T_m: is the mechanical torque applied to the motor.

T_e: is the electromagnetic torque produced by the motor.

T_L: is the Load torque

f: is the viscous friction coefficient.

J: is the moment of inertia.

θ_r: is the rotor angle or rotor postion.

V_α and V_β: are the alpha and beta components of the voltage vector.

I_α and I_β : are the alpha and beta components of the current vector.

θ: is the electrical angle between the reference frame and the A-phase.

ρ: is the density of water (1000kg/m3).

g: the acceleration due to gravity (9.8 m/s^2).

H: pressure head (in meters).

Q: flow rate (m3/s).

T_p: torque (Nm)

Ω: pump speed or velocity (rad/s)

K_{pc}: proportionality constant

Pr: the rated input power to the pump (watt)

Ωr: the pump rated speed (rad/s)

m: is the number of particles in PSO algorithm

X_i and V_i: the position and velocity of particle i.

k: the number of iterations.

w: the particle inertia weight.

c_1 and c_2: learning factors

r_1 and r_2: random numbers between (0,1).

i_{sa}, i_{s_β} : stator current components.

Ψ_{sa,s_β} : stator flux components.

σ: the leakage coefficient.

p: the number of poles pairs.

Ψ_s, Ψ_r: stator and rotor flux vectors.

δ: angle between the stator and rotor flux vectors

h_{Te}: the hysteresis band of torque.

P_{best}: personal best.

G_{best}: global best.

General Introduction

The process of transitioning in energy sources is currently underway on global scale, with the exponential increase of the use of renewable energy solutions in both developed and developing countries, this resulted in creating local value and jobs and increase in community resilience. Due to its abundance, cleanliness, and longevity, solar energy has become one of the most widely used sources of renewable energy for industrial and residential electricity needs. It is free, has no carbon footprint and emits no pollutions [1].

The availability of water has become more crucial than ever before. The demand for water grows along with the world's population. The need for water to irrigate land, which will then produce more food, as well as clean water for drinking purposes, is crucial with coping in the world's population growth [2].

A source of energy to pump water is also a big problem in many developing countries. Developing a grid system is often too expansive because rural villages are frequently located too far away from grid lines. Depending on an imported fuel supply is difficult and risky, even if fuel is available within the country, transporting that fuel to remote rural villages can be difficult. There are no roads or supporting infrastructure in many remote villages where transporting by animal is still common. To overcome this issue, the use of renewable energy is attractive for water pumping applications in rural areas of many developing countries such as photovoltaic (PV) pumps [2].

Water pumping systems based on photovoltaic technology are good solutions for rural areas where access to the grid power lines can be difficult and expansive [3]. Thus, these systems are more reliable than those based on diesel pumps, because they require less maintenance [4]. However, the performance of a PV generation system is influenced by three factors which are irradiation, nature of load, and atmospheric temperature [5]. To improve these drawbacks, maximum power point tracking techniques are introduced to maximize the output power of the PV whatever the weather condition [6].

The main purpose of MPPT is to extract the MPP from the panel. However, it is hard to do the task under abnormal conditions, for instance partial shading conditions results in multiple peaks in the P-V curve which make it difficult for conventional MPPT techniques to extract the maximum power. As a solution, the metaheuristic-inspired optimization algorithms are suggested. They have been widely applied in Maximum Power Point Tracking (MPPT)

algorithms for photovoltaic (PV) systems. These algorithms aim to extract the maximum available power from the PV panels by continuously adjusting the operating point to track the maximum power point (MPP) under varying environmental conditions. The metaheuristic algorithms that are going to be used in our work is the Particle Swarm Optimization (PSO) technique, and the Grey Wolf Optimization technique (GWO).

The aims of the work

In this work, a single stage stand-alone induction motor-driven solar water pumping system is presented and designed in such a way that regardless of the amount of solar irradiation. The pump's power flow remains consistent. For maximum power extraction from the PV array, maximum power point tracking (MPPT) techniques are used, one of these techniques is the P&O, which is the famous control strategy due to its simplicity. However, this technique has limited performance under abnormal conditions. Therefore, the PSO and grey wolf optimization techniques are introduced as an MPPT techniques for PV system under partial shading conditions. The speed and torque of the induction motor are controlled using direct torque control (DTC), this method involves calculating an estimate flux and torque based on the instantaneous measurement of voltage and current of the motor.

The main contributions of the work are:

-Design of photovoltaic single stage PV water pumping system.

-Performing a double function voltage source inverter to drive the motor-pump and extract the maximum power point.

-Presentation of different MPPT algorithms such as P&O algorithm, Particle Swarm Optimization, Grey Wolf Optimization.

Work organization:

- **Chapter 1:** This chapter provides background information and a board overview of photovoltaic and solar water pumping systems, including different categories based on the power source and water source.
- **Chapter 2:** In this chapter we present the design and modeling and the components of the stand-alone solar water pumping system.
- **Chapter 3:** In this chapter we present the control of the whole system, starting by mentioning the MPPT algorithms and their flowcharts. Following that, we will discuss the DTC control strategy of the induction motor used to drive the centrifugal pump.
- **Chapter 4:** in this chapter different simulation results of the overall system have been presented and discussed.

Chapter 1:
Theoretical Background

1.1 Introduction

Worldwide energy demand is increasing, to meet social and economic development and human welfare and health. Renewable energy source can meet many times the present world energy demand. Solar photovoltaic (PV) energy is promising, due to its clean and quiet operation [7].

Photovoltaic technology is today the most well-known and commonly installed solar technology in the world [8]. The efficiency and effectiveness of PV array technologies have increased as semiconductors technology has developed. It has shown to be an innovator in delivering electricity to secluded areas that transmission networks fails to reach. PV array electricity also provides other benefits, such as simple installation, low maintenance requirements [9].

For a significant portion of the world's rural population where no access to the grid is available, pumping water which naturally requires energy is a basic necessity. Considering that the majority of this rural population resides in the warm tropical or subtropical regions. The use of Solar Energy is a desirable method of meeting these essential energy needs [10].

The water pumping systems can be classified in two types, hybrid and stand-alone each comes with advantages and drawbacks. Although the stand-alone SWP have low maintenance cost, eco-friendly and easy to install, it has the disadvantage of low effectiveness and low output power when the weather is cloudy or during nights. In some of the current literature, a pumped storage system and the installation of a battery storage system have been suggested as potential solutions to this issue. However, such systems would need more room and cost more money up front [11].

1.2 Solar Energy

Solar Photovoltaic energy (PV) is gaining global acceptance because photovoltaic energy emits significantly less carbon dioxide than fossil fuels, it aids in reducing climate change. As an energy source, solar PV has certain distinct benefits: once installed, it produces no pollution, no noise, quiet operation and emit nor greenhouse gasses [12].

Solar photovoltaic modules are highly dependable, long-lasting, and low-noise electricity-generating devices. They combine solar cells to maximize their production. Fuel for a solar cell is entirely free. For the proper operation of a PV system, just the sun's energy is required. A typical photovoltaic cell has an efficiency of 15%, meaning it can convert 1/6 of solar energy into electricity. Photovoltaic systems do not have moving parts and do not release pollutants into the atmosphere. Solar cell production uses several tens of times less energy per unit than fossil fuel technologies do, which results in less carbon dioxide being released into the atmosphere [13].

Photovoltaic are best known as a method for generating electric power by using solar cells to convert energy from the sun into a flow of electrons by the photovoltaic effect.

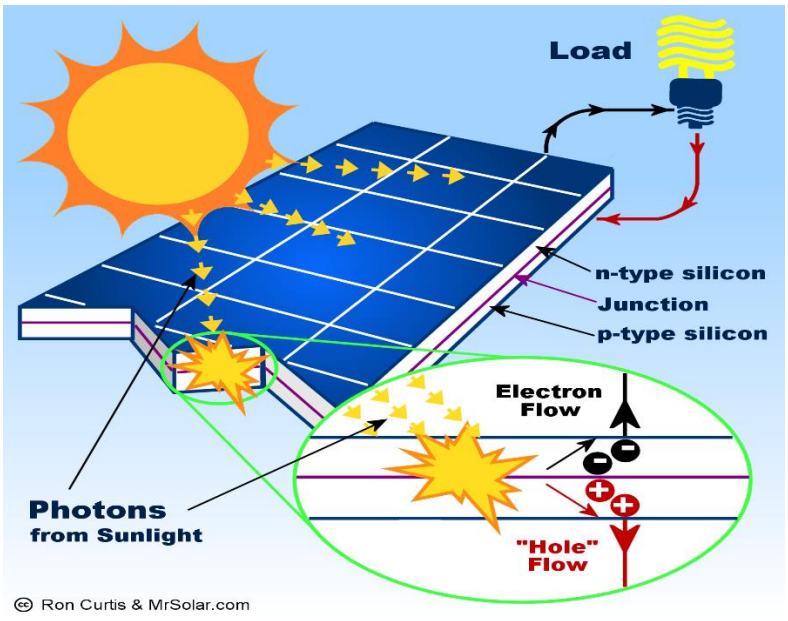

Figure 1.1 Photovoltaic energy transformation

1.3 Solar Water Pumping System Background

One potential use for a solar PV production system has come into focus: solar water pumping. Remote regions that receive large amount of irradiation can greatly benefit from it. By providing for the daily need for water, it would contribute to raising the level of living [14].

PV panels and pumps are the two key elements that make up a solar-powered water pumping system. The solar cell is the smallest component of a PV panel. Each solar cell contains two or more layers of semiconductor material that have been properly prepared to generate direct current (DC) power when exposed to light [15]. Basic configuration of SWPS is show in **Figure 1.2**

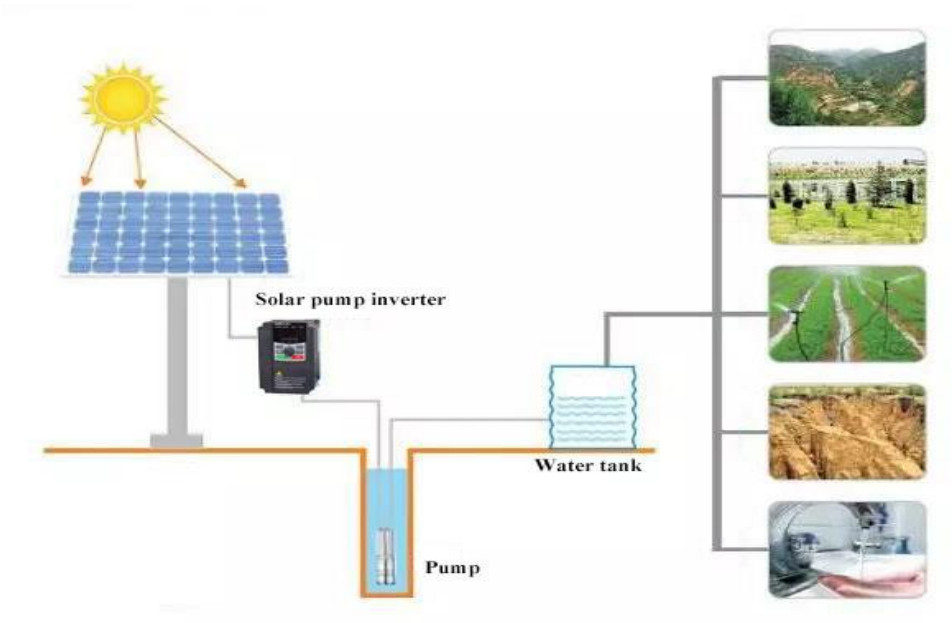

Figure 1.2 The basic configuration of SWPS.

1.3.1 Solar Water Pumping Configurations

There are various solar water pumping system kinds, and depending on the technique of classification, we can tell them apart as follows:

1.3.1.1 Power Source Based SWPS

Solar water pumping systems can be classified into two types, a standalone SWPS which its energy comes only from the PV panel only and it's highly dependent on the weather and irradiance, the second type is the hybrid SWPS which generally have a backup source of

energy in the absence of the sun or during night. When choosing the best system for a given application, many different aspects must be taken into account.

- **Stand-Alone Configuration**

Solar energy is the only power source in a standalone SWPS. It consists of a controller connecting a pump assembly to a PV array. The solar panels in a stand-alone solar system are not connected to a grid; rather, they are used to charge a bank of batteries during the day so that they can be used at night when the sun's energy is insufficient. In places without a public grid, stand-alone solar power systems have been used for a very long time.

Additionally, because standalone mode is so dependent on weather, it has the disadvantages of an intermittent power source and unreliable water pumping. Additionally, the water-pumping system (WPS) is not used at all at night and only partially during inclement weather. To increase the WPS's applicability and dependability, these weaknesses must be addressed by many different solutions, one of them is installing battery storage system [16].

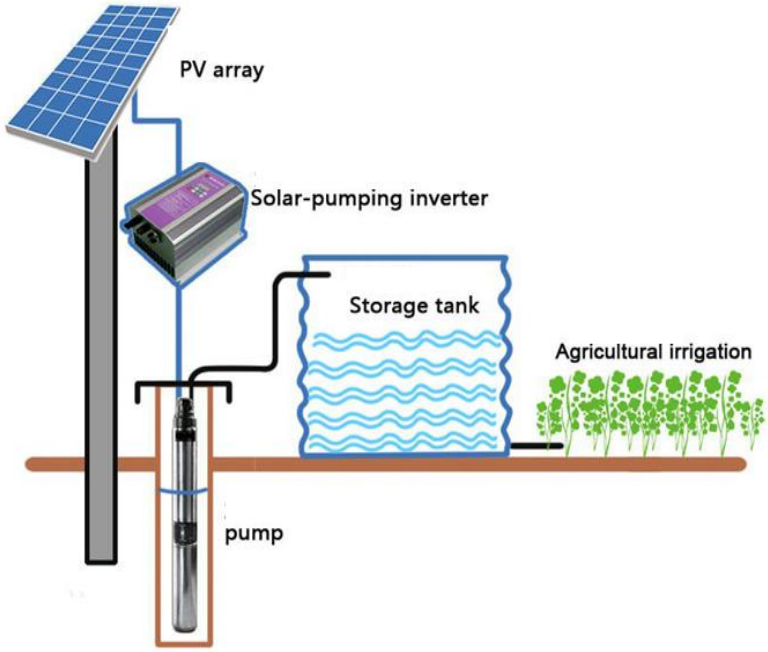

Figure 1.3 Schematic of stand-alone PV water pumping system.

The batteries keep charging and discharging in accordance with the presence of solar insulation, ensuring full water discharge in all operational circumstances. The battery's drawbacks, such as its high system complexity, high maintenance costs, and short lifespan, have, however, prompted experts to consider alternative options [17].

Installing a storage tank alongside the pumping equipment is one method to reduce dependency on unpredictable weather. Water can be kept in the storage tank when sunlight is present without the requirement for water pumping. The water can be utilized if the WPS as a whole is required to shut down owing to a lack of sunlight. On the other side, the installation of a storage tank requires some extra space compared to a bank of batteries [18].

- **Hybrid Configuration**

A hybrid PV water pumping system combines photovoltaic (PV) technology with another sources of power such as diesel generators and grid-connected PV systems. The stand-alone system may have a drawbacks of inconsistent water pump due to weather conditions, the hybrid systems help pumping consistent water all the time weather by using diesel generators to ensure the continuity of the pump, or connecting the system to the grid if it's available in the area. A schematic of hybrid solar water pumping system is shown in **Figure 1.4.**

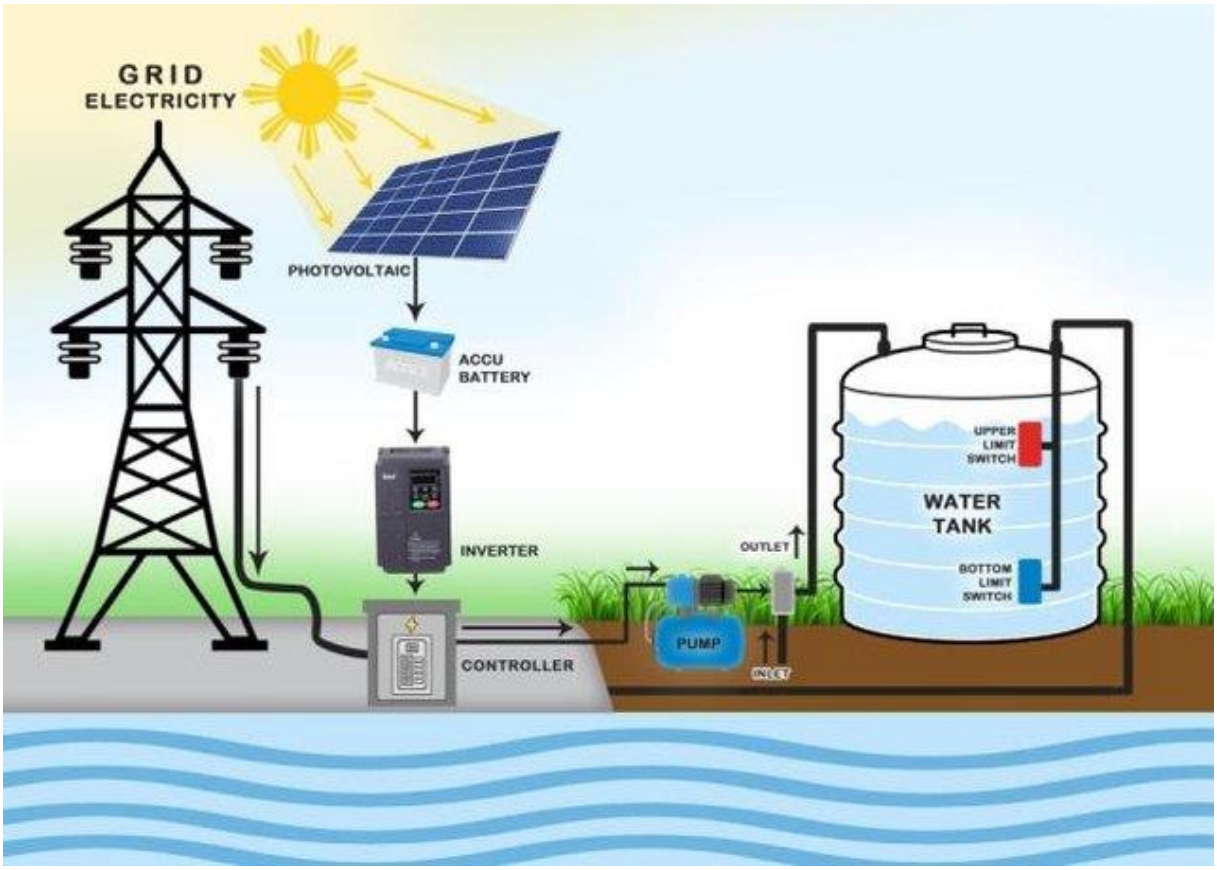

Figure 1.4 Schematic of hybrid solar PV water pumping system.

Table 1.1 we're going to highlight some of advantages and disadvantages between hybrid configuration and stand-alone configuration.

Configuration Type	Advantages	Disadvantages
Stand-Alone SWPS	-Reliance on solar energy. -Environmentally friendly. -Low maintenance requirements. -Suitable for remote areas.	-Limited water pumping capacity on cloudy days or during nighttime. -No backup power source, so water pumping ceases when sunlight is insufficient. -No power supply during system maintenance or repair.
Hybrid SWPS	-Reliable water supply even during low sunlight periods. -Increased water pumping capacity compared to standalone systems. -Utilizes solar energy as the primary power source, reducing reliance on fossil fuels.	-Higher initial investment cost compared to standalone systems. -Additional components and complexity in system design and operation. -Additional operational considerations for managing multiple power sources

Table 1.1 comparison between SWP configurations.

1.3.1.2 Based On Type of Pump (Water Source)

SWPS can be based on the type of pump used depending where the source of water is located, generally water is located in a surface area and deep under the ground.

- **Submersible Configuration**

In a centrifugal submersible water pump, the DC or AC motor is kept in a waterproof enclosure which is directly connected to the pump. The pump and motor together placed under the water. In the submersible solar water pump system, water is generally drawn from a bore well or in some cases a surface water source using a floating platform.

- **Surface Configuration**

In surface configuration the pump is installed at ground level, generally the source of water for surface configuration is lake, tank, dam or river, it contains a section pipe connecting the inlet to the water source and delivery pipe connecting the output to the delivery pipe.

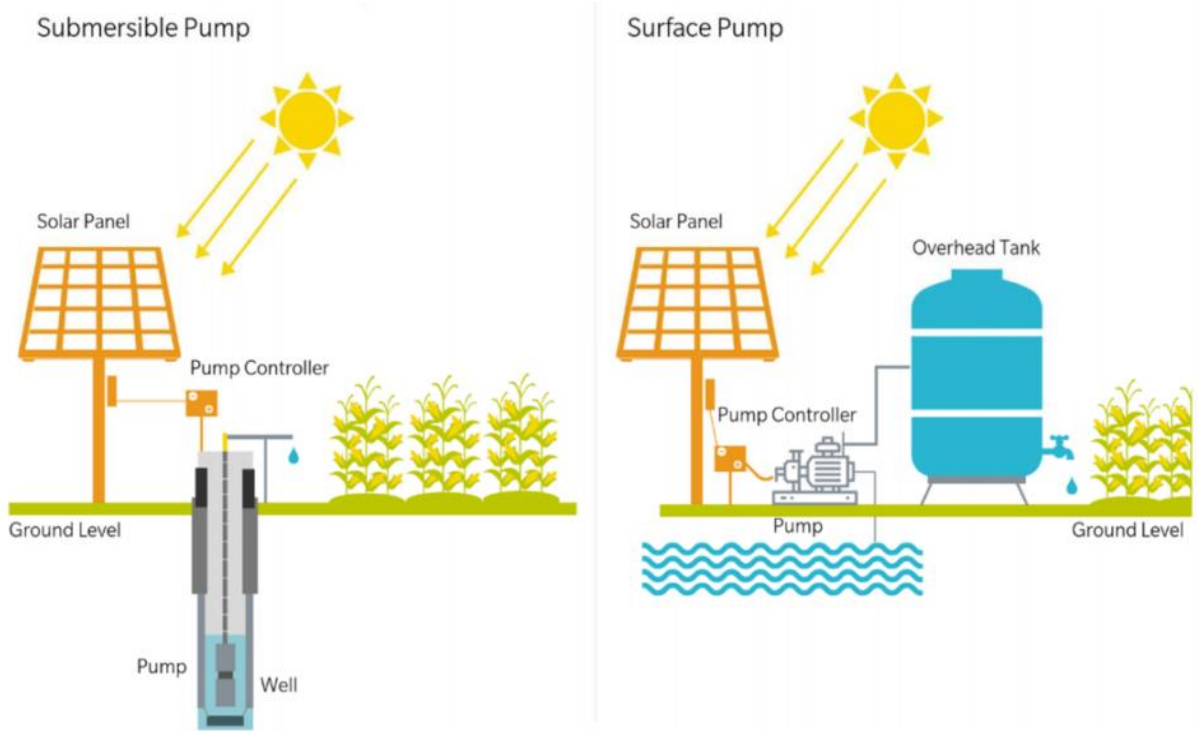

Figure 1.5 Submersible pump & Surface pump SWPS configuration.

1.3.1.3 Based On Type of Motor Used

The motor in SWPS is the heart of the system, it's the power that rotate the pump, all types of motor can be used to drive a pump weather its DC motors or AC motors each come with its advantages and disadvantages, based on motor type we can classify the SWPS into:

A) Based On DC Motors

There are two types of DC motors, the conventional dc motor and the brushless dc motor and they are as follow:

- **Conventional DC Motor (Brushed DC Motor)**

The brushed DC motor uses the carbon brushes to transfer electricity from the PV array to the shaft of the motor. The brushes require frequent replacement as they deteriorate with time. This comes with the increase of the maintenance cost, also it has the sparking occurring at the brushes resulting in damaging the motor and risk of failure [19].

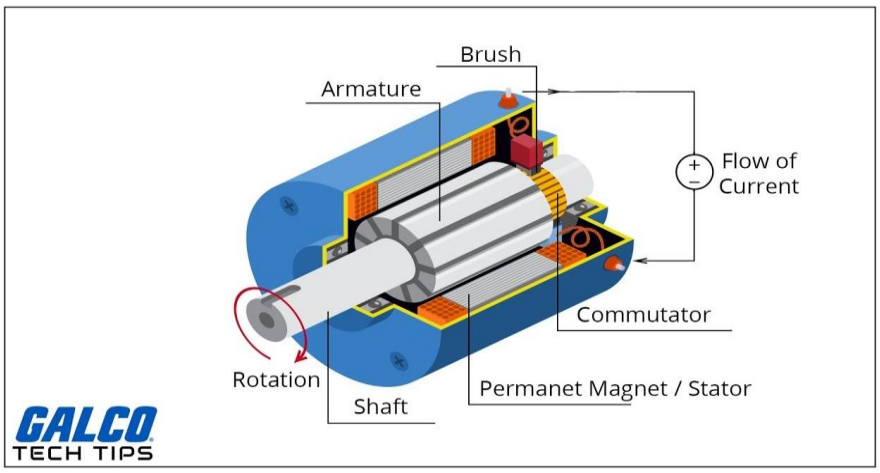

Figure 1.6 Brushed DC motor parts.

- **Brushless DC Motor (BLDC)**

A BLDC is used in solar pumping systems to overcome the prior limitations of the conventional DC motor. It is the most sophisticated motor among the DC motors. With its better performance, great torque characteristics, good medium and low-speed torque characteristics, high starting torque, modest starting current, and robust overload capacity, BLDC motors can unquestionably compete with any other motor for pumping applications. One drawback of the BLDC is that it can't achieve high speed because it is limited by the mechanical strength of the assembly between the rotor yoke and the permanent magnet [20].

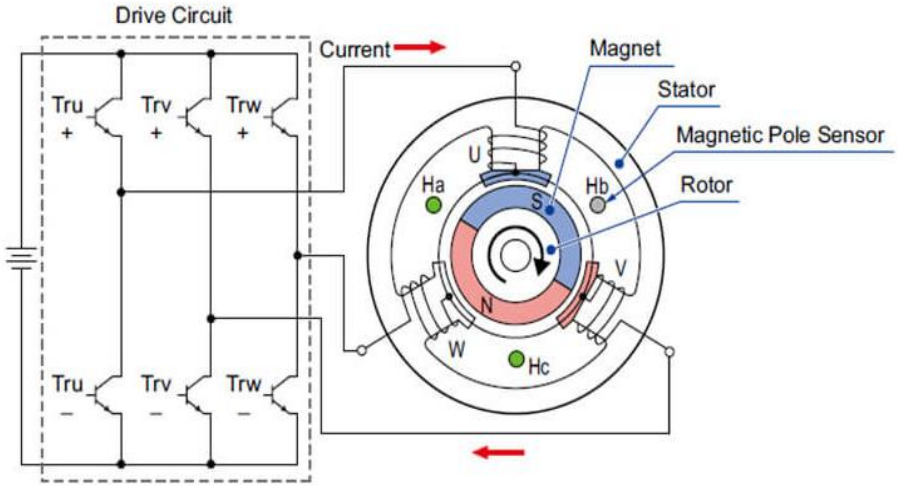

Figure 1.7 simplified model of brushless DC motor.

B) Based On AC Motors

The AC motors comes in two types the asynchronous motor (induction motor) and the synchronous motor, in this part both of them will be described briefly:

- **Induction Motor**

Overall, the industry, the induction motor (IM) is the most used motor due to its easy operation. The induction motor got attraction from the SWP developers over the DC motors due to its low cost, simplicity, robustness, durability and low maintenance. They can start directly for the line and can operate at variable speeds and loads. However, induction motors (IM) have some drawbacks, such as low efficiency, power factor, and torque. They also produce more heat, noise, and slip than synchronous motors.

Controlling these motors is challenging because the IM operates slower than the synchronous speed at all times. Furthermore, accurate motor parameter estimates, sophisticated modeling, and complicated control circuitry are required for the real-time implementation of these motor drives [21].

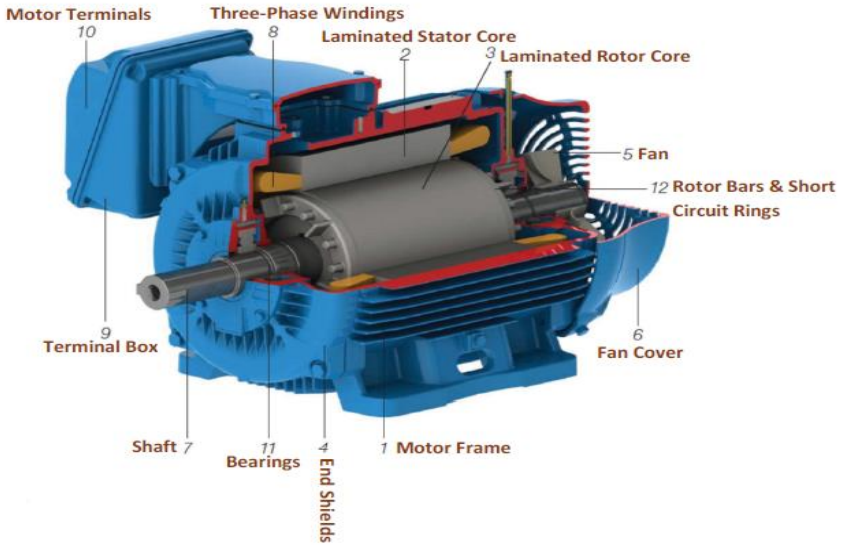

Figure 1.8 basic parts of induction motor (IM).

- **PMSM Motor**

PMSM motors are commonly utilized in water pumping systems due to their efficient operation, precise speed control, compact size, and reliability. These motors consist of a rotor with permanent magnets and a stator with windings, generating a rotating magnetic field that interacts with the magnets to produce motion. PMSM motors offer the ability to achieve optimal power consumption, ensuring efficient pumping of water. They also enable accurate regulation of water flow and pressure, making them suitable for applications with specific water

requirements. Their compact and lightweight design allows for easy installation in space-limited environments. Additionally, PMSM motors operate without brushes, reducing the need for maintenance and enhancing their overall reliability. In water pumping systems, PMSM motors contribute to improved water management and system performance.

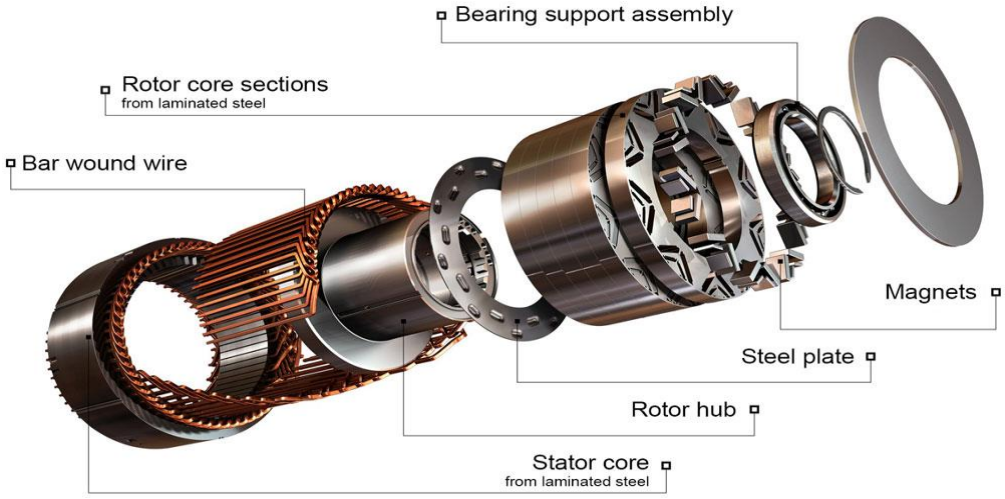

Figure 1.9 construction of PMSM motor.

- **Choosing Between S Motors**

Choosing between the motors depends on several factors, such as the required speed, torque, power, load, and application. Generally, synchronous motors are more suitable for applications that need constant speed, high power, or precise control, such as pumps, compressors, or conveyors. Induction motors are more suitable for applications that need variable speed, low power, or simple operation, such as fans, blowers, or mixers. You should also consider the availability, cost, and maintenance of the motor and its components.

Table 1.2 shows advantages and disadvantages of each type of motor used in SWP

Motor Type	Advantages	Disadvantages
DC Motor	-simple and efficient design -Directly compatible with PV panels and batteries. -Good torque control and starting capabilities.	-Requires additional control circuitry. -Limited power range for larger applications. -Limited speed control capabilities.
AC Motor	-Wide availability and variety of options. -Greater power range for larger applications. -Better speed control capabilities.	-Requires an inverter for compatibility with PV panels and batteries. -Lower efficiency compared to DC motors. -Higher initial cost.

Brushless DC Motor	-Higher efficiency compared to brushed DC motors. -Improved reliability and longer lifespan. -Better speed and torque control capabilities.	-Requires additional control circuitry. -Higher initial cost. -Limited availability of repair services.
PMSM	- No sparks, safer in explosive environments -Smooth for low and high-speed performance -Good torque and power factor control. -Runs with/without position encoders	- Expansive - Risk of demagnetization

Table 1.2 comparison between advantages, disadvantages of each type of motor in PV SWP.

1.4 Description of the Single-Stage Stand-Alone Solar Water Pumping System

The stand-alone SWPS comes with the difficulty to pump water during night times and when the sun is unavailable, but as a solution a water storage tank is used to save water when the pumping process isn't available. In our work the single stage was chosen based on the following.

- **Comparison Between Single-Stage And Double-Stage SWPS**

AC solar water pumping systems can be categorized as double-stage and single-stage systems. In a double-stage system, DC-DC and DC-AC converters are connected in cascade, resulting in increased cost and complexity. To overcome these challenges, a single-stage system is employed for direct conversion of solar photovoltaic (SPV) power to drive the water pump using an inverter. The single-stage system offers advantages such as cost reduction, lower switching losses, and decreased complexity, making it an appealing choice for solar water pumping applications [22].

Table 1.3 gives general comparison between the two different configurations.

Aspect	Double-stage system	Single-stage system
System complexity	Double-stage systems involve the connection of DC-DC and DC-AC converters in cascade, leading to increased complexity due to the presence of multiple conversion stages.	-Single-stage systems offer simplicity as they directly convert SPV power to drive the water pump using an inverter, resulting in reduced complexity and a more straightforward system design.
Cost	Double-stage systems tend to be costlier compared to single-stage systems due to the additional components required, such as the DC-DC converter.	Single-stage systems are typically more cost-effective as they eliminate the need for an intermediate DC-DC converter, resulting in reduced equipment and installation costs.
Efficiency	Double-stage systems may experience slightly lower overall efficiency due to the additional conversion stages, which introduce additional losses.	Single-stage systems can achieve higher overall efficiency since they involve direct conversion from SPV power to AC power without the need for intermediate conversion stages.
Flexibility	Double-stage systems offer greater flexibility in terms of voltage matching between the solar panels and the water pump, as the DC-DC converter can enable voltage adjustment.	Single-stage systems may have limited flexibility in terms of voltage matching, as the direct connection of solar panels to the inverter may require careful selection of compatible components.
Maintenance	Potential for additional maintenance	Lower maintenance requirements

Reliability	Double-stage systems may require additional maintenance due to the presence of the DC-DC converter and the complexity of the system. However, the redundancy provided by separate converters can enhance system reliability.	Single-stage systems generally have lower maintenance requirements and can offer reliable operation, benefiting from the simplicity of the system design.
Scalability	Double-stage systems can offer greater scalability, as the presence of a DC-DC converter allows for easier integration of additional solar panels or batteries.	Single-stage systems may have more limitations in terms of scalability, as the direct connection to the inverter may require careful consideration of the system's capacity and compatibility.

Table 1.3 general comparison between double-stage and single-stage SWPS

In summary, Double-stage AC solar water pumping systems provide flexibility in voltage matching and scalability but come with increased complexity and cost. On the other hand, single-stage systems offer simplicity, cost-effectiveness, higher efficiency, and reduced maintenance requirements, making them an attractive choice for many solar water pumping applications.

The water pump can be driven by any motor mentioned above, each come with its advantages and drawbacks. A typical configuration of a single stage stand-alone water pumping system is shown in **Figure 1.10** it shows the power transfer from the PV feeding an induction motor driven pump.

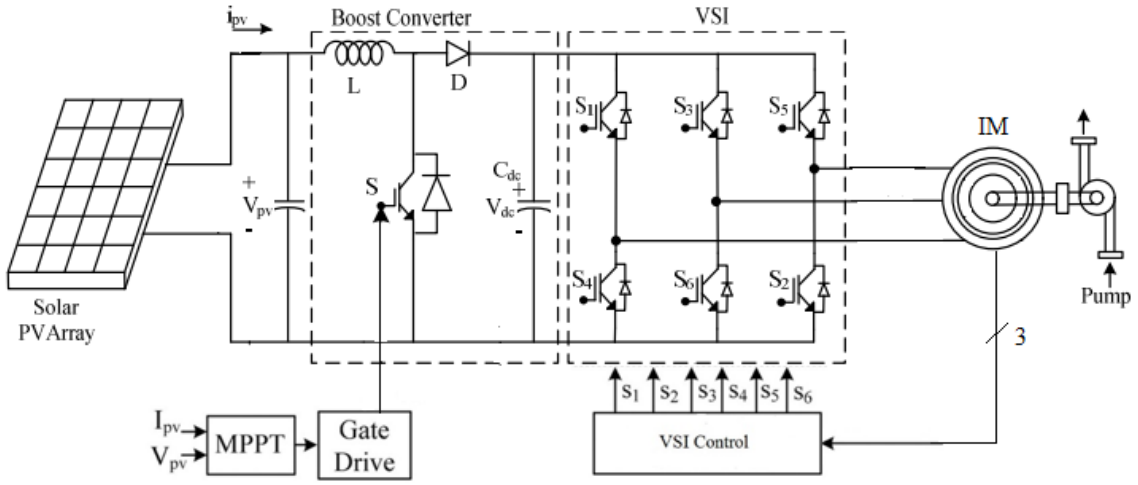

Figure 1.10 Schematic of a double-stage stand-alone SWPS [23].

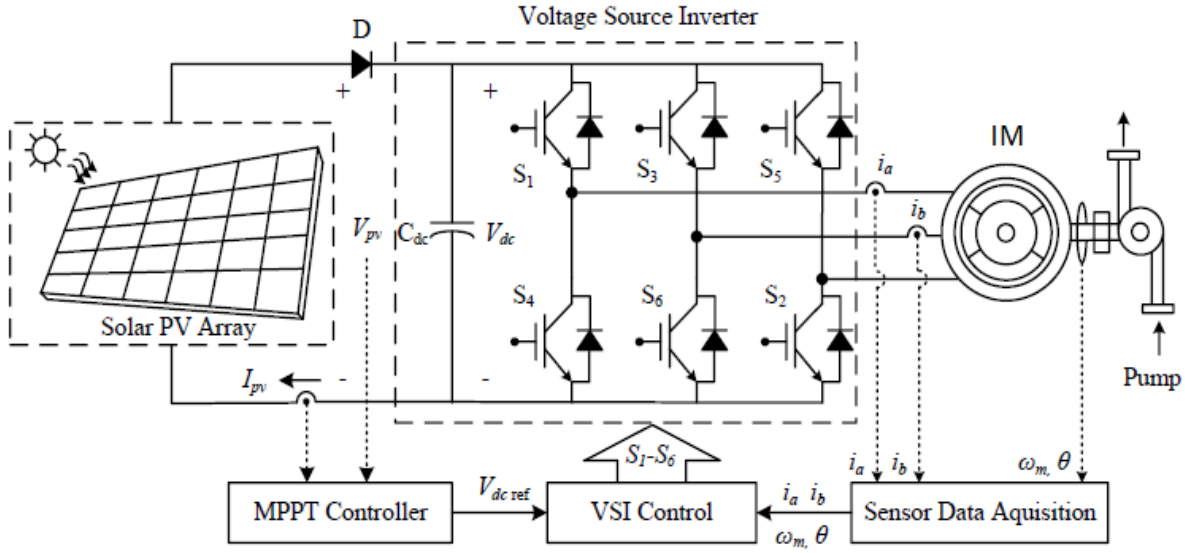

Figure 1.11 schematic of a single-stage stand-alone SWPS [24].

The configuration for SWP system, is shown in **Figure 1.11**. This system comprises of (from left to right) SPV array, a three-phase voltage source inverter (VSI), an induction motor (IM) and a water pump. A diode (D) is used between SPV array and VSI to stop the flow of any reverse current into SPV array. The SPV array consists of appropriate number of series and parallel combination of SPV modules. As the photons strike the surface of the SPV array, electrical energy is generated. This generated electrical energy is fed to the DC link of VSI. The VSI will generate three-phase voltages to feed motor pump [24].

1.5 Conclusion

This chapter covered a general introduction about solar PV energy, the significance of SWPS, particularly in rural or desert places, has also been demonstrated. A background about solar water pumping system has been introduced and classified based on water source, motor type used, and weather its stand-alone configuration or hybrid configuration. A comparison between stand-alone and hybrid configuration has been done in a table mentioning advantages and disadvantages of configuration. Also, a comparison between each motor type that will be used in SWPS is covered. At last, a schematic of the single-stage stand-alone SWPS configuration has been presented and described.

Chapter 2:
System description and configuration

2.1 Introduction

In this chapter, a modeling of photovoltaic stand-alone single-stage pumping system will be discussed, each component will be discussed individually to have best understanding on how it works and to understand the working principle of the whole system. We start from the power source, the power will be generated from the PV array only. In general two stage power conversions are employed using DC-DC boost converter between solar-PV panel and a Voltage Source Inverter (VSI) [25]. However, a single-stage conversion for the PV systems finds more interest for AC drive applications [26]. The solar PV panel is connected to voltage source inverter through an intermediate DC bus capacitor. The AC terminals of VSI are feeding the Induction Motor drive. The single stage inverter will perform maximum power point tracking of (MPPT) of the PV panel. The motor will be coupled directly to the centrifugal pump.

2.2 Photovoltaic Modeling

2.2.1 Working Principle of Solar Cells

A photovoltaic cell is comprised of many layers of materials, each with a specific purpose. The most important layer of a photovoltaic cell is the specially treated semiconductor layer. It is comprised of two distinct layers p-type and n-type, and is what actually converts the Sun's energy into useful electricity through a process called the photovoltaic effect. On either side of the semiconductor is a layer of conducting material which "collects" the electricity produced. Note that the backside or shaded side of the cell can afford to be completely covered in the conductor, whereas the front or illuminated side must use the conductors sparingly to avoid blocking too much of the Sun's radiation from reaching the semiconductor. The final layer which is applied only to the illuminated side of the cell is the anti-reflection coating. Since all semiconductors are naturally reflective, reflection loss can be significant. The solution is to use one or several layers of an anti-reflection coating to reduce the amount of solar radiation that is reflected off the surface of the cell [27].

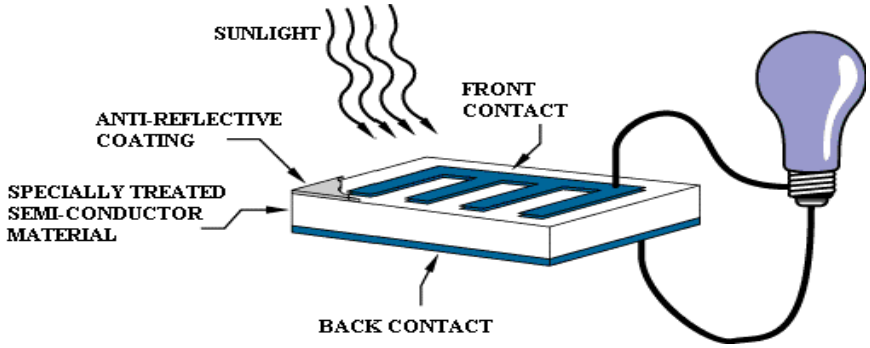

Figure 2.1 The basic operation of a PV cell [28].

The photovoltaic effect is a process that generates voltage or electric current in a photovoltaic cell when it is exposed to sunlight. These solar cells are made of a p-n junction, which is formed by joining two different types of semiconductors an n-type and a p-type together. By joining these two types of semiconductors, an electric field is formed in the region of the junction as electrons move to the positive p-side and holes move to the negative n-side. Positively charged particles move in one direction while negatively charged particles move in the opposite direction due to this field [29]. Light is composed of photons, which are simply small bundles of electromagnetic radiation or energy. When light of a suitable wavelength is incident on these cells, energy from the photon is transferred to an electron of the semiconducting material, causing it to jump to a higher energy state known as the conduction band. In their excited state in the conduction band, these electrons are free to move through the material, and it is this motion of the electron that creates an electric current in the cell.

2.2.2 Modeling of The PV Generator

A single PV cell will not produce enough current or voltage for any application, therefore the cells are added together in parallel or series configurations to produce solar cell modules, several modules in parallel or series will produce a PV array which is usable in many applications.

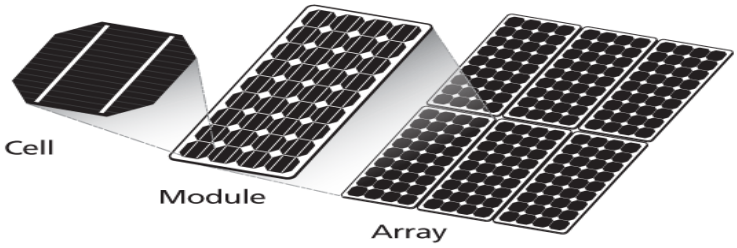

Figure 2.2 illustration of PV cell, Module and Array.

2.2.2.1 Solar Cell Model

A single solar cell can be represented as a component of an electrical circuit. It contains a p–n junction called as a diode, a photocurrent generator represented a generation of current from light and two resistors, one is arranged in series R_s and another one is in parallel R_{sh} which described the Joule effect and recombination losses. Then this combination is called as a single diode solar cell model [30].

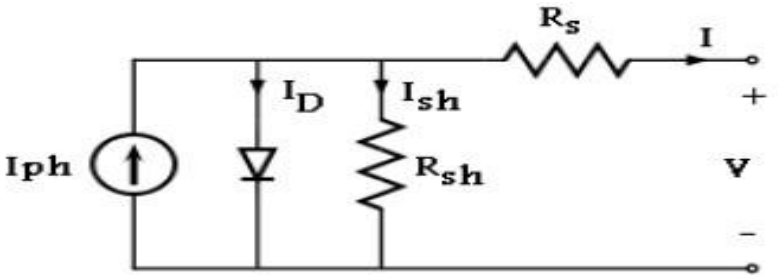

Figure 2.3 Single diode solar cell model.

The basic semiconductor theory is showed in the following equations:

$$I_{ph} = I_D + I_{sh} + I \tag{2.1}$$

$$I = I_{ph} - I_o * exp\left[\left(\frac{q(V + IR_s)}{AKT_c}\right) - 1\right] - \left[\frac{V + R_s}{R_{sh}}\right] \tag{2.2}$$

$$V = \frac{AKT_c}{q} ln\left[\frac{I_{ph} + I_o - I}{I_o}\right] - IR_s \tag{2.3}$$

Equation (2.2) can be written as:

$$I = I_{ph} - I_o * exp\left[\left(\frac{(V + IR_s)}{AV_t}\right) - 1\right] - \left[\frac{V + R_s}{R_{sh}}\right] \tag{2.4}$$

$$V_t = \frac{N_s KT_c}{q} \tag{2.5}$$

Where:

I: Cell output current in Amps
I_{ph}: The Photocurrent, is the current produced by the incident light and function of irradiation level and junction temperature in Amps
I_D: The diode current modeled by the equation for a Shockley diode in Amps
I_o: The saturated reverse current or leakage current in Amps
q: Electron charge (1.602 × 10-19 C).
K: Boltzmann constant (1.38 x 10 -23 J/°K)
V: Cell output voltage, (V)
T_o: Cell operating temperature, °K

A: The diode ideality factor
$R_{s,\,cell}$: Series resistance of the cell, Ohm
$R_{sh,cell}$: Shunt resistance of the cell, Ohm
V_t: Thermal voltage, V
N_s: Number of series cells

2.2.2.2 Solar Module Model

In order to increase solar cell voltage the solar cells have to be connected in series, and in order to increase the current it must be connected in parallel.

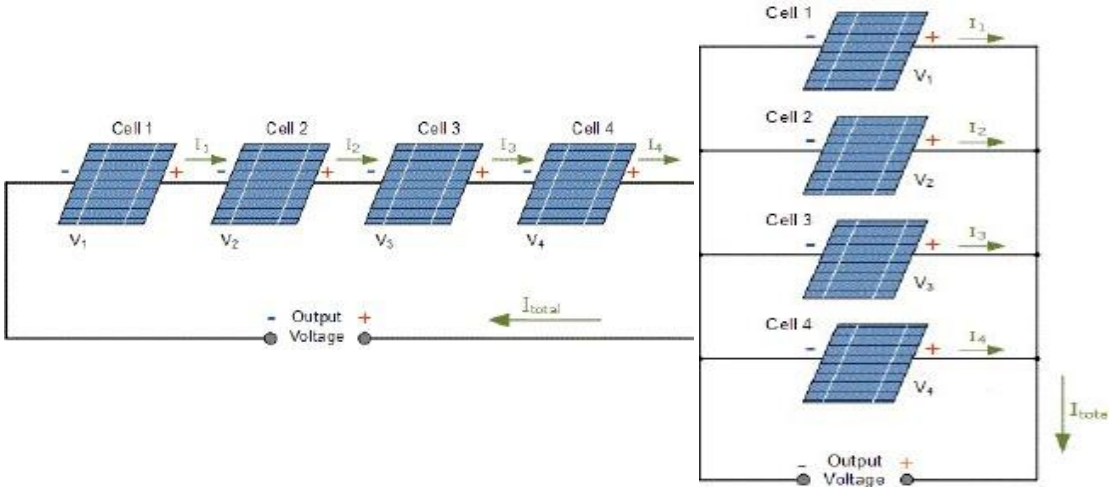

(a) (b)

Figure 2.4 PV cells connection (a) in series (b) in parallel.

The output voltage increases in the series connection ($V_{out}=V_1+V_2+V_3+V_4...$), and the output current increases in the parallel connection is ($I_{out}=I_1+I_2+I_3+I_4...$).

The sum of the module's shunt resistance (R_{sh} Module) and series resistance (R_s Module) for Np cells in parallel and Ns cells in series is equal to:

$$R_{sh,module} = \left(\frac{N_p}{N_s}\right).R_{sh,cell} \qquad (2.6)$$

$$R_{s,module} = \left(\frac{N_s}{N_p}\right).R_{s,cell} \qquad (2.7)$$

Where:

$R_{sh,module}$: Total shunt resistance in the photovoltaic module, Ohm.
$R_{s,module}$: Total series resistance in the photovoltaic module, Ohm.
$R_{sh,cell}$: Shunt resistance in one photovoltaic cell, Ohm.

$R_{s,cell}$: Series resistance in one photovoltaic cell, Ohm.
N_s: Number of cells in series
N_p: Number of cells branches in parallel

The following variables are then written as functions of a single cell's parameters, and this is the approximation approach, which determines the module current [31]:

$$I_{sc,module} = N_p . I_{sc,cell} \quad (2.8)$$

$$V_{oc,module} = N_s . V_{oc,cell} \quad (2.9)$$

Where:
$I_{sc,module}$: Total short circuit current of the photovoltaic module, A.
$V_{oc,module}$: Total open circuit voltage of the photovoltaic module, V.
$I_{sc,cell}$: Short circuit current of one photovoltaic cell.
$V_{oc,cell}$: Open circuit voltage of one photovoltaic cell.

2.2.2.3 Solar Array Model

A PV system typically has arrays of modules joined together. V_{array} is the terminals voltage of the array, and the current is denoted as I_{array}, the current is denoted as follows:

$$I_{array} = \sum_{i=0}^{M_p} I_i \quad (2.10)$$

Assuming that each module is identical and that each module receives the same amount of sunlight, the array current is as follows:

$$I_{array} = M_p . I_M \quad (2.11)$$

The sum of the voltages in the array is the summation of each module connected in series in one branch.

2.2.3 Design of the PV Array

The parameters of photovoltaic (PV) systems voltage and current are significantly influenced by temperature and light exposure. It's essential to comprehend these effects to maximize the efficiency and output of PV systems.

The influence of temperature on the semiconductor characteristics of PV cells results in changes in the voltage and current output of PV systems. While the output of current tends to increase as temperatures increase, the output of voltage decreases. This is primarily because PV module short-circuit current (I_{sc}) and open-circuit voltage (V_{oc}) temperature coefficients. The voltage and current output of PV systems are also influenced by irradiation. Higher

irradiation levels result in an increase in both voltage and current output, while lower irradiation levels have opposite effect.

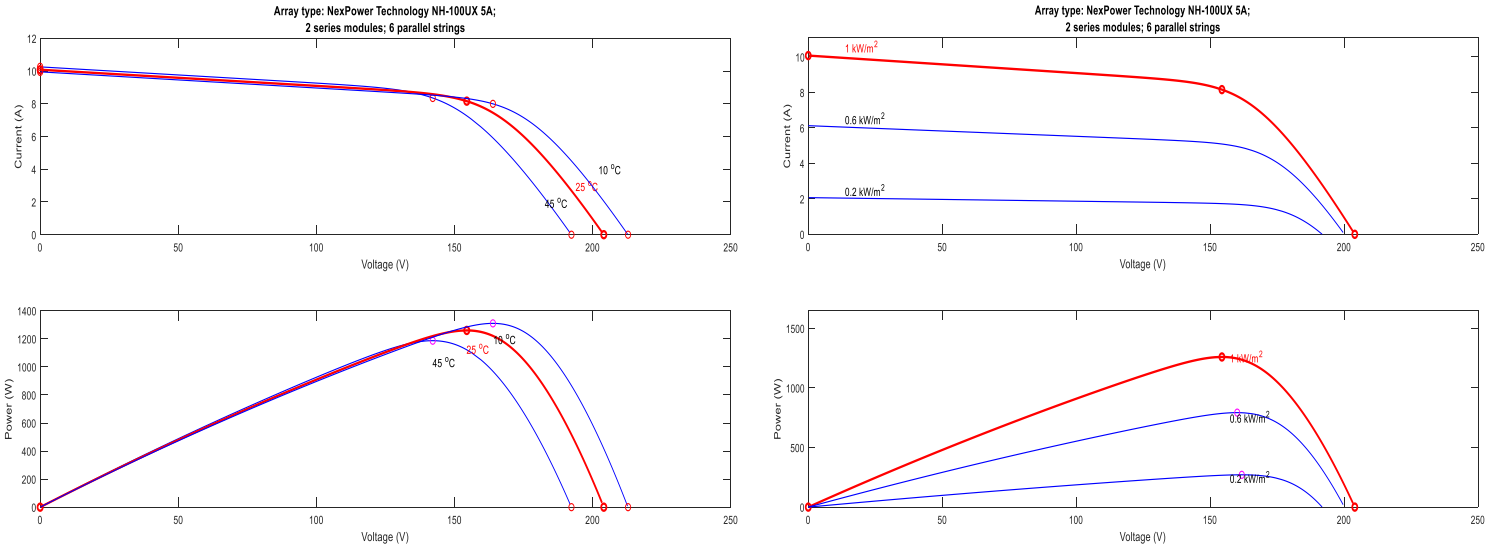

Figure 2.5 The effect of ambient temperature and irradiation variations on P-V and I-V curves.

A 1.1 kW IM motor pump is powered by 1.26 kW PV array. The converter and motor pump power losses are considered. At the standard condition (1000W/m², 25 ^{o}C) the parameters are estimated. To design a PV array of needed capacity. PV module- **NexPower Technology NH-100UX 5A** with mpp voltage 77.2V and mpp current 1.36A is chosen. The power versus voltage (P-V) and the current versus voltage (I-V) characteristics of the PV model under STC are shown in **Figure 2.6.**

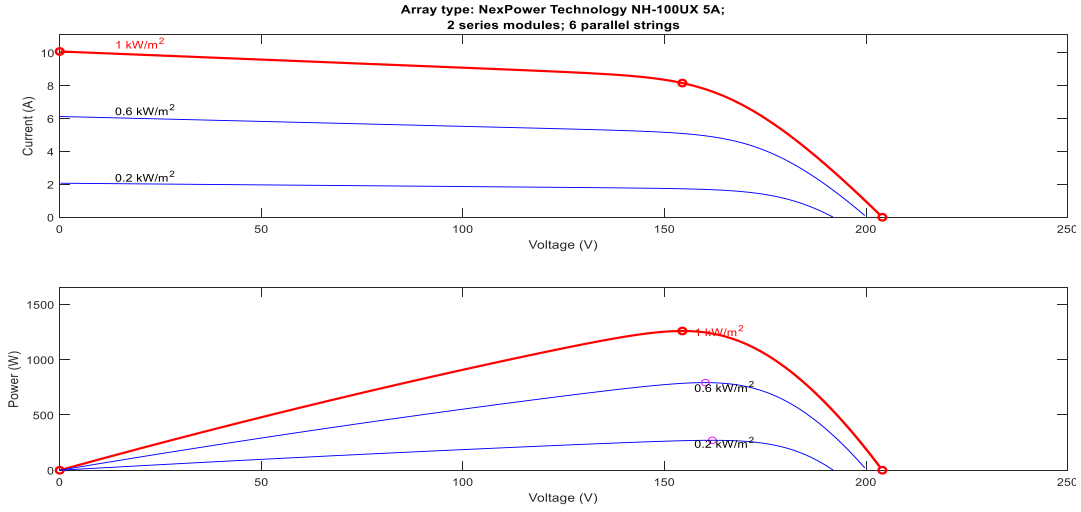

Figure 2.6 P-V and I-V characteristics of PV module- NexPower Technology NH-100UX 5A.

The full specification of the PV array is shown in the appendices.

The PV array consist of 3 PV modules, each module consist of 2 panels in parallel and 2 panels in series.

2.2.4 Solar Module Under Partial Shading Effect

When a solar cell module is subjected to partial shading, it experiences non-uniform illumination, resulting in different levels of current generation across the cells. This condition can lead to significant power losses and hotspots, making it crucial to employ techniques such as bypass diodes or maximum power point tracking (MPPT) algorithms to mitigate these effects and optimize overall system performance.

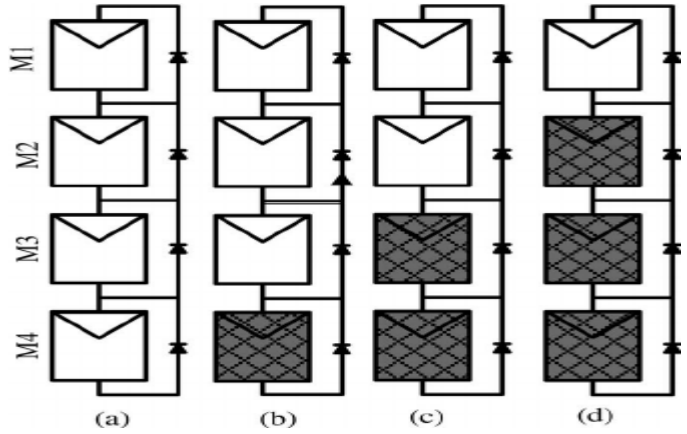

Figure 2.7 PV array under different partial shading conditions.

Under partial shading, PV arrays experience varying levels of sunlight due to shading. Consequently, this leads to a mismatch between the modules, a decrease in power production, and the occurrence of hotspots. In order to fulfill the power requirements of the load, PV panels are commonly interconnected in parallel or series. However, when partial shading occurs due to shadows from objects like trees, buildings, poles, or even cloud movement in large-scale PV systems, the power output of the PV array experiences a significant reduction. Partial shading arises from uneven distribution of sunlight, resulting in the appearance of multiple peaks on the power-voltage (P-V) curve and causing power losses. The specific pattern of shading, the positioning of shaded modules, and the configuration of the array are important factors influencing the extent of these power losses [32]. **Figure 2.8** shows panels under partial shading:

Figure 2.8 PV panels under shading.

When a PV panel is under shading hotspot phenomena will occur, it is when a PV panel consume power instead of generating power, the power loss due to the hotspot effect is primarily caused by increased resistive losses within the cell. The higher temperature can result in higher series resistance, leading to increased voltage drop across the resistive elements in the cell. This voltage drop leads to power dissipation in the form of heat rather than contributing to the overall power output of the PV system. These effects can damage the system by reducing efficiency, degradation of the system, and causing safety risks. To prevent hotspots, it is crucial to minimize shading on PV panels and ensure the panels are installed and maintained properly. Technologies such as bypass diodes, which allow current to bypass the shaded or damaged cells, can also help mitigate the effects of partial shading and reduce the risk of hotspots [33].

- **Bypass Diodes:**

A bypass diode is a device used in solar photovoltaic (PV) arrays to protect partially shaded PV cells from fully operating cells in full sun within the same solar panel when used in high voltage series arrays. Bypass diodes are connected in reverse bias between a solar cell's positive and negative output terminals and have no effect on its output [34]. They are used in parallel with either a single or a number of photovoltaic solar cells to prevent the current flowing from well-exposed to sunlight solar cells overheating weaker or partially shaded solar cells by providing a current path around the bad cell. Bypass diodes are usually placed across groups of solar cells, rather than one per cell, as this is more cost-effective [35] . Bypass diodes are wired within the PV module and provide an alternate current when a cell or panel becomes shaded or

faulty [36]. They are also used to eliminate the hot-spot phenomena which can damage PV cells and even cause fire if the light hitting the surface of the PV is not distributed evenly.

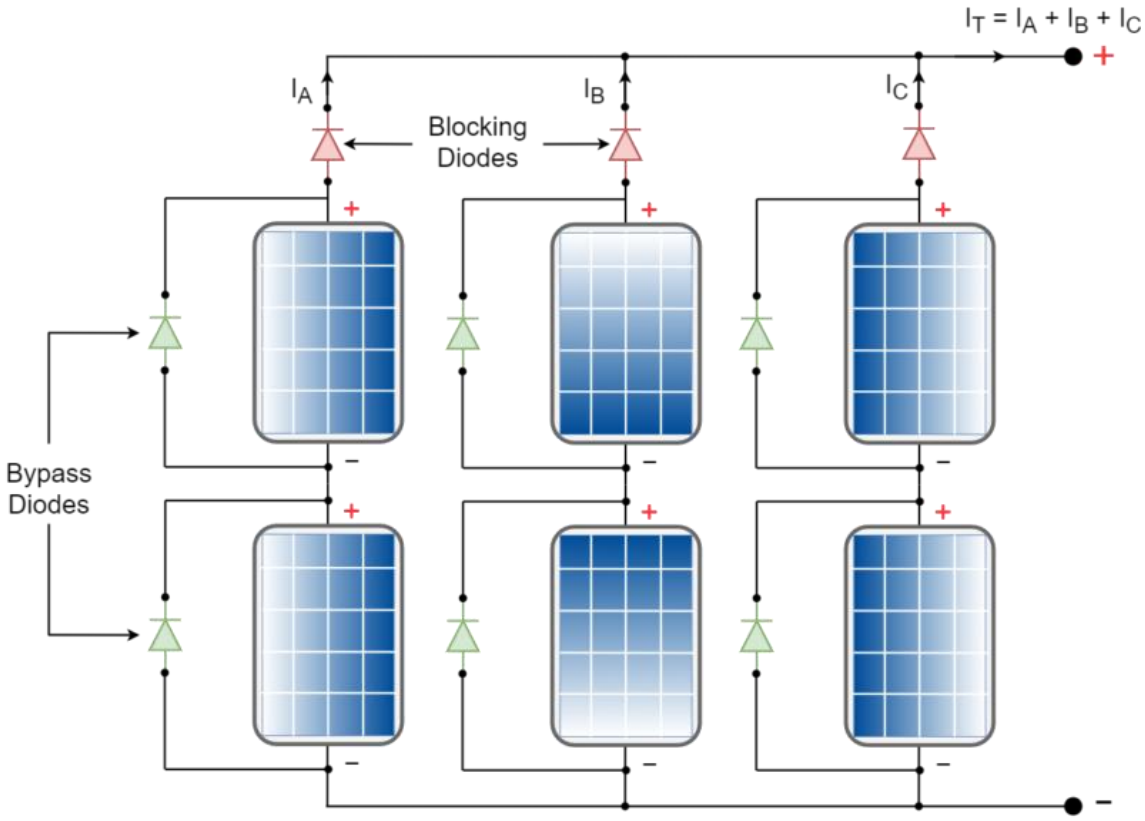

Figure 2.9 Bypass and blocking diodes in a PV system [37].

The presence of bypass diodes in an array, as depicted in **Figure 2.10**, results in different characteristics compared to an array without these diodes. The inclusion of bypass diodes creates an alternative path for current flow, causing cells within a module to carry varying currents when subjected to partial shading. Consequently, as illustrated in **Figure 2.11**, the power-voltage curve exhibits multiple peaks, including a global maximum that represents the true maximum power point (MPP) and other local peaks. Unfortunately, the presence of multiple peaks in the PV characteristic poses a significant challenge, as many conventional maximum power point tracking (MPPT) algorithms struggle to differentiate between local and global maxima [34].

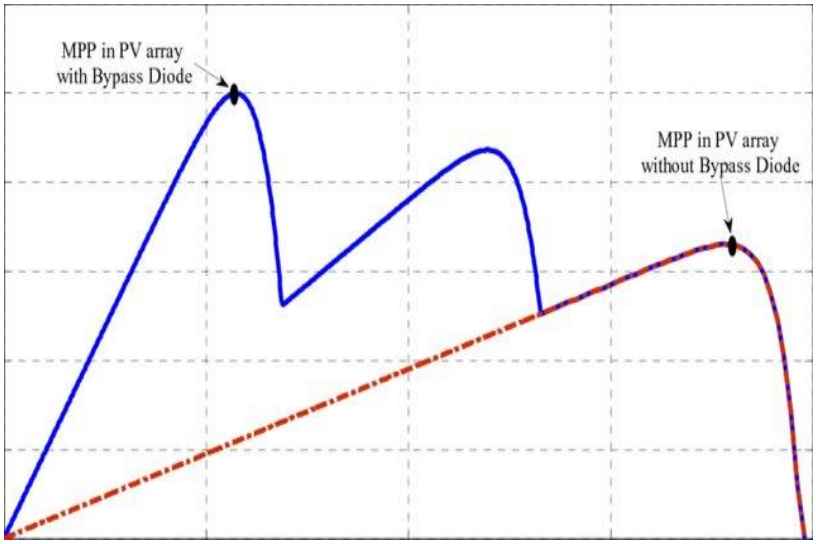

Figure 2.10 PV characteristic curves under partial shading with and without bypass diodes [38].

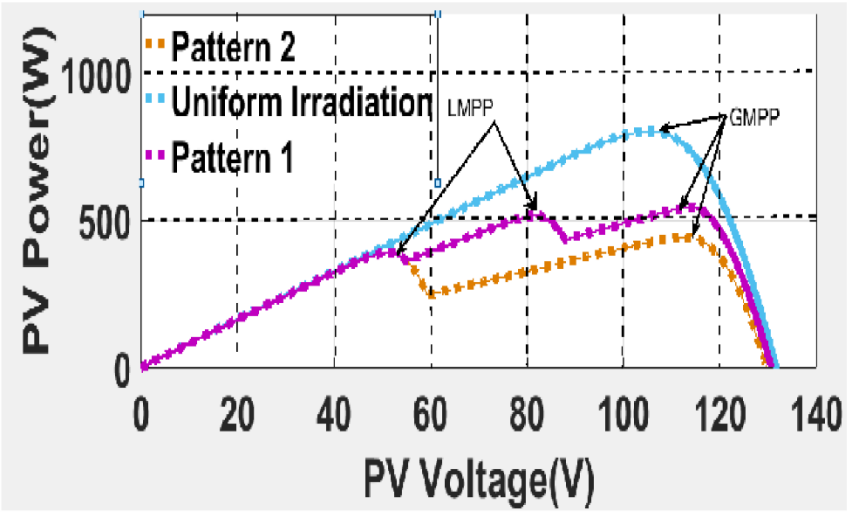

Figure 2.11 PV characteristic curves for uniform and non-uniform irradiations [39].

It is important to note that bypass diodes are different from blocking diodes, which are wired in series with the solar cell or panel and prevent current from flowing in the reverse direction [40].

2.3 Voltage Source Inverter VSI

Many different applications require DC/AC converters [41]. A voltage source inverter is used to convert dc to ac output. It consists of six switches, IGBTs and MOSFETs are the two most suitable switching components for these inverters. Due to simplicity in their structure and ability to handle the voltage by keeping the system stable, they are preferred utmost in the industry and for commercial purpose due to their support in uninterruptible power supply

applications. Various types of control systems are implemented by the researchers to improve their performance, robustness and stabilization, compensating the power losses and lowering the THD value [42]. They are widely utilized to provide controlled frequency and ac voltage magnitudes utilizing different pulse width modulation (PWM) techniques in motor drives, active filters, and unified power flow controllers in power systems and uninterrupted power supplies [43].

The standard three-phase inverter shown in **Figure 2.12,** it has six switches the switching of which depends on the modulation scheme:

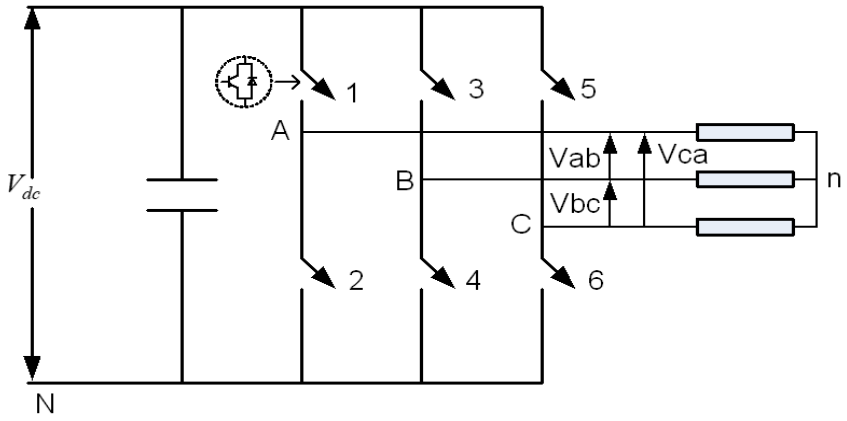

Figure 2.12 Three-phase VSI circuit

The inverter has eight switching states given in **Table (2.1).** The VSI is constrained by Kirchoff's voltage (KVL) and current (KCL) rule in that both devices in a leg cannot be turned on simultaneously in order to prevent shorting of the DC link capacitor. However, it does permit the adjacent legs to be cut shorter. Thus, the nature of the two switches in the same leg is complementary [44].

$$S_{11}+S_{12}=1 \qquad (2.12)$$

$$S_{21}+S_{22}=1 \qquad (2.13)$$

$$S_{31}+S_{32}=1 \qquad (2.14)$$

Two of the eight switching states represented in Table (2.1) result in ac line voltages of zero at the output. The ac line currents in this situation freely cycle through the upper or lower components. There are no 0 ac output line voltages in the remaining states. The inverter alternates between states to produce a certain voltage waveform. The resulting ac output line voltages are made up of the discrete voltage values V_{DC}, 0 and $-V_{DC}$ [45].

S_{11}	S_{12}	S_{31}	V_{ab}	V_{bc}	V_{ca}
0	0	0	0	0	0
0	0	1	0	$-V_{DC}$	V_{DC}
0	1	0	$-V_{DC}$	V_{DC}	0
0	1	1	$-V_{DC}$	0	$-V_{DC}$
1	0	0	V_{DC}	0	$-V_{DC}$
1	0	1	V_{DC}	$-V_{DC}$	0
1	1	0	0	V_{DC}	$-V_{DC}$
1	1	1	0	0	0

Table 2.1 The switching states in three-phase inverter.

The state selection to generate the given waveform is achieved by modulating technique that ensures the use of only the valid states.

$$\frac{V_{DC}}{2}(S_{11} - S_{12}) = V_{an} + V_{nN} \quad (2.15)$$

$$\frac{V_{DC}}{2}(S_{21} - S_{22}) = V_{bn} + V_{nN} \quad (2.16)$$

$$\frac{V_{DC}}{2}(S_{31} - S_{32}) = V_{cn} + V_{nN} \quad (2.17)$$

Adding the equations from 2.15 to 2.17 gives equation 2.18 as follow:

$$\frac{V_{DC}}{2}(S_{11} + S_{21} + S_{31} - S_{12} - S_{22} - S_{32}) = V_{an} + V_{bn} + V_{cn} + 3V_{nN} \quad (2.18)$$

As we are dealing with balanced voltages $V_{an} + V_{bn} + V_{cn} = 0$ equation 2.18 becomes:

$$\frac{V_{DC}}{6}(2S_{11} + 2S_{21} + 2S_{31} - 3) = V_{nN} \quad (2.19)$$

Substituting for V_{no} in Equations 2.15 to 2.17 gives:

$$\frac{V_{DC}}{3}(2S_{11} - S_{21} - S_{31}) = V_{an} \quad (2.20)$$

$$\frac{V_{DC}}{3}(-S_{11} + 2S_{21} - S_{31}) = V_{bn} \quad (2.21)$$

$$\frac{V_{DC}}{3}(-S_{11} - S_{21} + 2S_{31}) = V_{an} \quad (2.22)$$

The source of the equations above was taken from educational website [46].

There are eight possible positions from the combinations of switching states. Six are active vectors (V1, V2 … V6) and two are zero vectors (V0, V7) [47]. These eight switching states are shown as space vectors in **Figure 2.13**:

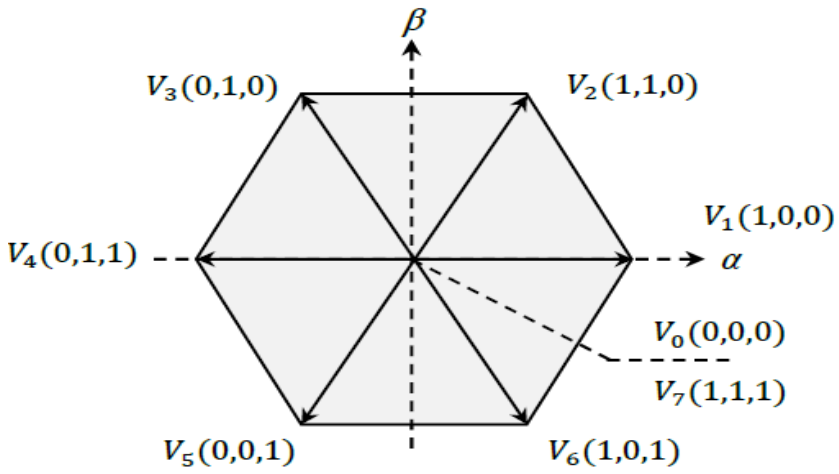

Figure 2.13 VSI Voltage vectors in the complex plane.

2.4 Induction Motor

An induction motor, also known as an asynchronous motor, is an AC electric motor in which the magnetic field of the stator winding is used to electromagnetically induct the electric current into the rotor necessary to produce torque. Therefore, it is possible to construct an induction motor without electrical connections to the rotor. Either a wound type rotor or a squirrel-cage type rotor can be used in an induction motor [48].

Induction motors' relationship between mechanical and electrical speeds is that the electrical speed is determined by multiplying the mechanical speed by the number of poles divided by half. An induction motor's working speed is determined by the input power frequency and the number of magnetic poles inside the motor. The number of poles determines the synchronous speed for an electric induction motor, and because of the slip between synchronous and actual speed, the speed of an induction motor is always a little slower than synchronous speed. The electric motor's physical design and the frequency of the voltage supply both affect how fast it rotates [49] [50].

2.4.1 Modeling Hypotheses

The modeling of the AC electrical machine generally relies on several hypotheses. The central proposition is to assume that the magnetomotive forces produced by the stator and rotor windings follow a sinusoidal distribution in the air gap when a constant current passes through them. Additionally, it is assumed that the air gap of the machine is evenly thick. We disregard any notching effects that may produce spatial harmonics.

Other hypotheses about the physical behavior of the materials also are expressed:

- Linear magnetic characteristic (no saturation).
- The skin effect is not taken into account.
- Temperature effect, hysteresis phenomenon, and eddy currents are neglected.

2.4.2 Mathematical Model of the Induction Motor

The mathematical model of an induction motor can be represented by a set of differential equations that describe its electrical and mechanical behavior. Additionally, the alpha-beta (α-β) model and used to simplify the representation of the motor's currents and voltages. Here is the mathematical model of an induction motor, along with the α-β model.

The mathematical model of an induction motor comprises equations that govern the electrical and mechanical dynamics of the motor. It contains of electrical equations and mechanical equations.

Voltage Equations:

$$\begin{cases} [V_{sabc}] = R_s[i_{sabc}] + \dfrac{d}{dt}[\psi_{sabc}] \\ [V_{rabc}] = 0 = [R_r][i_{rabc}] + \dfrac{d}{dt}[\psi_{rabc}] \end{cases} \quad (2.23)$$

Flux Equations:

$$\begin{cases} [\psi_{sabc}] = [L_s\lceil i_{sabc}] + [M_{sr}\lceil i_{rabc}] \\ [\psi_{rabc}] = [L_r][i_{sabc}] + [M_{sr}]^T[i_{sabc}] \end{cases} \quad (2.24)$$

Where:

$$[V_{sabc}] = \begin{bmatrix} V_{sa} \\ V_{sb} \\ V_{sc} \end{bmatrix}; [i_{sabc}] = \begin{bmatrix} i_{sa} \\ i_{sb} \\ i_{sc} \end{bmatrix}; [\psi_{sabc}] = \begin{bmatrix} \psi_{sa} \\ \psi_{sb} \\ \psi_{sc} \end{bmatrix}$$

$$[V_{rabc}] = \begin{bmatrix} V_{ra} \\ V_{rb} \\ V_{rc} \end{bmatrix}; [i_{rabc}] = \begin{bmatrix} i_{ra} \\ i_{rb} \\ i_{rc} \end{bmatrix}; [\psi_{rabc}] = \begin{bmatrix} \psi_{ra} \\ \psi_{sb} \\ \psi_{rc} \end{bmatrix}$$

The subscripts *s* and *r* refer to the stator and the rotor, respectively, and the indices *a*, *b*, and *c* refer to the three phases.

Equations 2.25 is the mechanical equations:

$$\frac{d\,\omega_m}{dt} = \left(\frac{1}{J}\right)(T_e - T_L - f\,\omega_m) \quad (2.25)$$

- **The Alpha-Beta Transformation**

The αβ transformation is used to convert the three-phase quantities (voltages, currents) to a two-phase reference frame aligned with the stator flux. We use Concordia transformation. The Concordia transformation matrix is given as equation (2.29):

$$C = \sqrt{\frac{2}{3}}\begin{bmatrix} 1 & -\frac{1}{2} & -\frac{1}{2} \\ 0 & \frac{\sqrt{3}}{2} & -\frac{\sqrt{3}}{2} \\ \frac{1}{\sqrt{2}} & \frac{1}{\sqrt{2}} & \frac{1}{\sqrt{2}} \end{bmatrix} \quad (2.26)$$

The dynamic equation's model of the induction motor which is dedicated for direct torque control is expressed below in Eq (2.27) and Eq (2.28). It can be written in the stator fixed reference frame (α, β) (stationary frame) by assuming the stator current and the stator flux as state variables.

$$\begin{cases} \frac{di_{sa}}{dt} = -\left(\frac{R_s}{\sigma L_s} + \frac{R_r}{\sigma L_r}\right) i_{s\alpha} - \omega_r i_{s\beta} + \frac{R_s}{\sigma L_s L_r}\Psi_{sa} + \frac{\omega_r}{\sigma L_r}\Psi_{s\beta} + \frac{1}{\sigma L_{.s}} V_{sa} \\ \frac{di_{s\beta}}{dt} = -\left(\frac{R_s}{\sigma L_s} + \frac{R_r}{\sigma L_r}\right) i_{s\beta} - \omega_r i_{sa} + \frac{R_s}{\sigma L_s L_r}\Psi_{s\beta} + \frac{\omega_r}{\sigma L_r}\Psi_{sb} + \frac{1}{\sigma L_{.s}} V_{s\beta} \end{cases} \quad (2.27)$$

$$\begin{cases} \frac{d\Psi_{sa}}{dt} = V_{sa} - R_s i_{sa} \\ \frac{d\Psi_{s\beta}}{dt} = V_{s\beta} - R_s i_{s\beta} \end{cases} \quad (2.28)$$

Where:

i_{sa}, $i_{s\beta}$ are stator current components.

$\Psi_{sa,s\beta}$ are stator flux components.

R_s, R_r are stator and rotor resistances.

L_s, L_r are stator and rotor inductance.

$\sigma = 1 - \frac{M_{sr}}{L_s L_r}$ is the leakage coefficient.

M_{sr} is the mutual stator-rotor inductance.

2.6 The Centrifugal Pump

These are the pumps used in irrigation systems by a wide margin. This specific solar pump spins the water quickly in a casing, chamber, or housing utilizing an impeller (a rotating element

that transmits motion in a device). Centrifugal force is the term for the spinning motion. The centrifugal pump's ability to pump water is due to this force. These solar centrifugal pumps may have a number of stages, during which the pressure of the water increases [51].

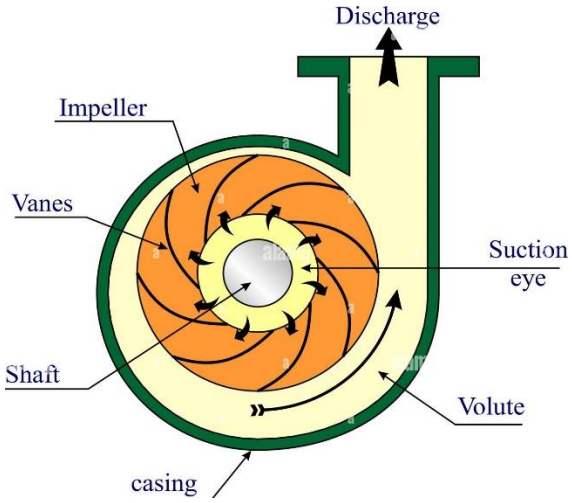

Figure 2.14 Centrifugal Pump.

-The efficiency of a centrifugal pump is given as:

$$\eta = \frac{P_{output}}{P_{input}} = \frac{P_{water}}{P_{shaft}} \quad (2.29)$$

The water input and output of a shaft are connected. The power supplied to the pump shaft is known as the shaft power, and the water power is computed using the formula below:

$$P_{water} = \rho g H Q \quad (2.30)$$

Where:

ρ: is the density of water (1000kg/m3).

g: the acceleration due to gravity (9.8 m/s2).

H: pressure head (in meters).

Q: flow rate (m3/s).

The pump torque can be expressed as:

$$T_p = Kpc.\Omega^2 \quad (2.31)$$

Where:

T_p: torque (Nm)

Ω: pump speed or velocity (rad/s)

K_{pc}: proportionality constant and it can be estimated as:

$$K_{pc}=P_r/\Omega_r^3 \quad (2.32)$$

Where:

P_r: the rated input power to the pump (watt)

Ω_r: the pump rated speed (rad/s)

- **The Affinity Laws**

To ensure the proper functioning of processes, it is essential to meet the hydraulic requirements of head and flow rate. The Affinity Laws provide mathematical relationships that enable the estimation of how variations in shaft speed (N) or impeller diameter affect the performance curves of a pump. These laws help us understand the impact of changes in pump parameters on its overall operation.

According to the Affinity Laws, when the impeller diameter remains constant, the flow rate (Q) of a pump is directly proportional to the speed, the head (H) is directly proportional to the square of the speed, and the required power (P) is directly proportional to the cube of the speed. These laws establish clear relationships between pump speed and its corresponding flow rate, head, and power requirements [51].

$$\begin{cases} \dfrac{Q_1}{Q_2} = \dfrac{\Omega_r}{\Omega_{rn}} \\ \dfrac{H_1}{H_2} = \left(\dfrac{\Omega_r}{\Omega_{rn}}\right)^2 \\ \dfrac{P_1}{P_2} = \left(\dfrac{\Omega_r}{\Omega_{rn}}\right)^3 \end{cases} \tag{2.33}$$

Where:

H_2, Q_2 and P_2 are the rated parameters of the pump at speed Ω_{rn}.

H_1, Q_1 and P_1 are the parameters of the pump at a speed Ω_r different from the rated speed.

2.7 Conclusion

The concluding section of this chapter provides a comprehensive overview of the functioning of each component within the system. It begins by offering a concise explanation of the operational principles of solar cells, followed by the presentation of the photovoltaic generator model and its unique characteristics. Additionally, the power converter utilized in the proposed pumping system is described, shedding light on its power circuits and specific attributes. Furthermore, the modeling process of the Induction Motor is elucidated. A general portrayal of the centrifugal pump is also included, highlighting its efficiency, torque equation, and the affinity laws which facilitate the estimation of variations in pump performance resulting from changes in shaft speed. Lastly, the system design is addressed, encompassing the selection of an appropriate PV generator.

Chapter 3:
Control of the System

3.1 Introduction

The control of the system constitutes of MPPT control of the VSI using different maximum power point tracking algorithms in normal condition and in partial shading condition, MPPT is used in order to improve the efficiency of the PV generator and to make the system operate at maximum power.

The speed control of the IM using the VSI, the Direct Torque Control technique is used to drive the induction motor. The primary focus of DTC is to achieve fast and accurate control of motor speed while maintaining good dynamic performance and high efficiency. In DTC, the motor's stator flux and electromagnetic torque are controlled by manipulating the voltage and frequency of the motor. This control is achieved through a combination of hysteresis comparators, which compare the actual values of torque and flux with their respective reference values, and a lookup table that determines the appropriate voltage vectors to be applied to the motor.

The P&O MPPT algorithm is going to be used under normal condition, it is a simple MPPT technique for PV systems. The Grey-Wolf MPPT technique is going to be used under normal condition and partial shading conditions, it allows the dynamic adjustment of the operating point of a solar panel and maximize the power output, and another technique particle swarm optimization technique is also going to be seen under normal condition and under partial conditions.

The flow chart of the Perturb and Observe (P&O) MPPT method remains largely the same for both single-stage and double-stage PV systems. The fundamental principle of the P&O algorithm, which involves perturbing the operating voltage and observing the corresponding change in power output, remains consistent. However, there can be some variations in the implementation details based on the specific configuration of the PV system. In a single-stage PV system, the P&O algorithm typically operates directly on the output of the solar panel. The perturbation and observation occur at the panel level.

3.2 Maximum Power Point Tracking Algorithms

MPPT algorithms play a vital role in photovoltaic (PV) applications due to the varying MPP of solar panels influenced by factors like weather conditions, shadowing, and temperature. Implementing an MPPT algorithm is essential for optimizing power extraction by dynamically adjusting the power extraction process. The convergence speed of the MPPT algorithm is a critical aspect as improving its rise time enhances system reliability, increases power extraction, and improves overall system efficiency [52].

3.2.1 Perturb and Observe (P&O)

The Perturb and Observe algorithm, also known as the hill climbing method, is an MPPT technique that relies on calculating the output power of a system. This algorithm introduces perturbations that cause changes in the system's output power. If the perturbation moves towards the maximum power point, the voltage is increased. Conversely, if the perturbation deviates from the maximum power point, the voltage is decreased. As a result, the voltage is modified, and this process persists until the maximum power point is attained [53] **Figure 3.1** shows our proposed P&O algorithm flowchart:

In P&O we start by initialization the values, we fix V_{ref} at lower voltage for the motor to accelerate with more stability, then we start the algorithm by scanning I_{pv}, V_{pv} and calculating P_{pv}, we let ∓ 2 without updating V_{ref} for more robust system. By setting V_{max} and V_{min}, we prevent V_{ref} from diverging causing slow response, more perturbance and V_{dc} from reaching the boundaries (0, Voc) which will lead to zero power.

When the output power increases, the panel voltage is modified in the same direction as the previous cycle, as depicted in **Figure 3.2**. Conversely, if the output power decreases, the panel voltage is adjusted in the opposite direction compared to the previous cycle. When the maximum power point (MPP) is attained, the output voltage will oscillate around the maximum operating voltage [55].

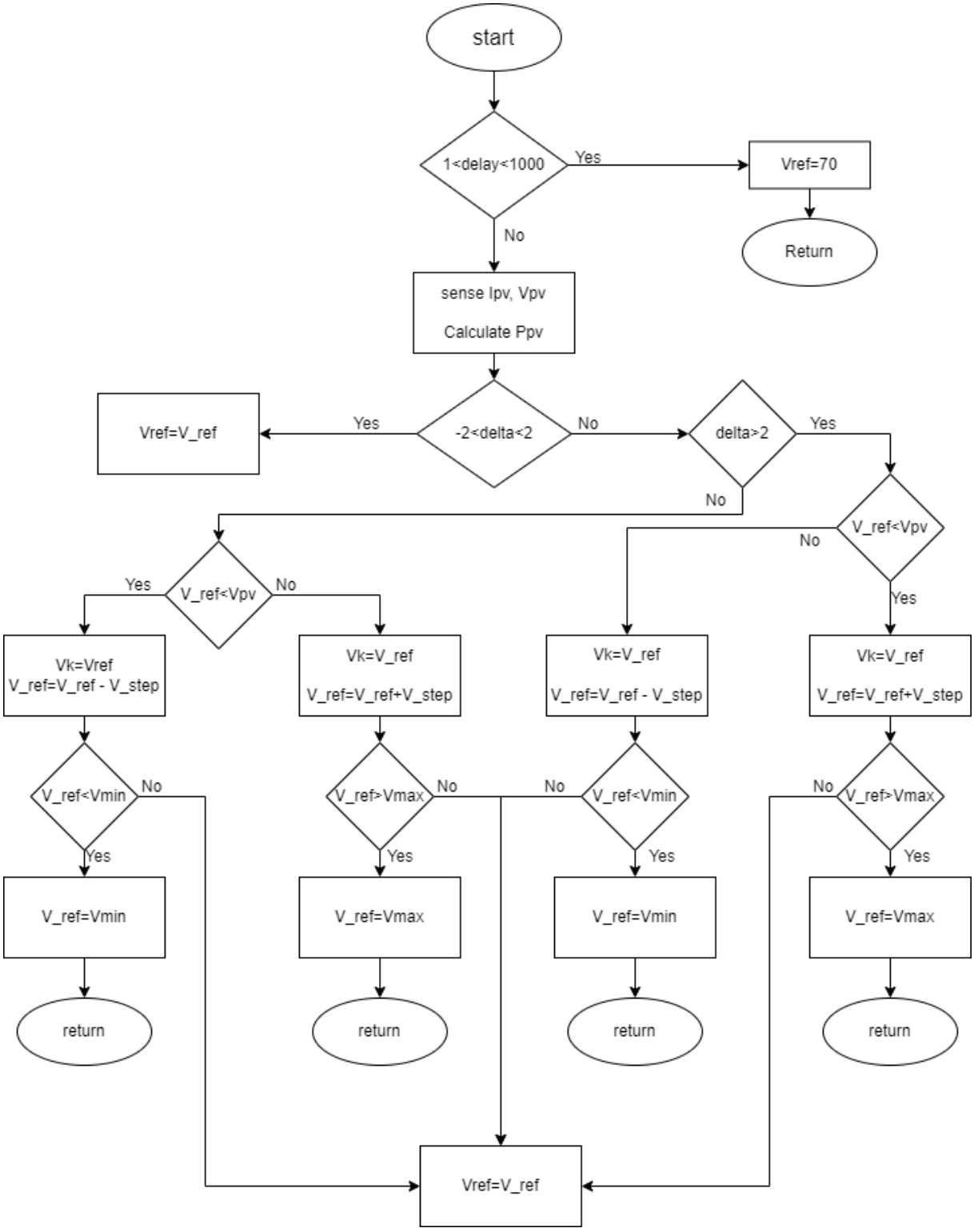

Figure 3.1 conventional P&O algorithm Flowchart [54].

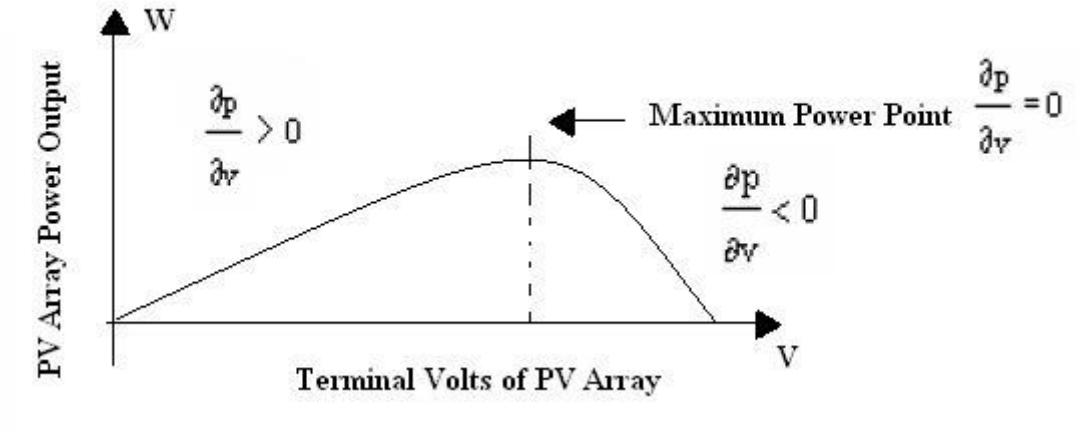

Figure 3.2 P-V characteristics of PV panel with MPP [56].

Furthermore, the P&O algorithm is extensively utilized as an MPPT method owing to its combination of performance and simplicity. However, it faces limitations in terms of speed and adaptability required to effectively track rapid transients amidst changing environmental conditions. While it is a straightforward and uncomplicated technique, the trade-off between accuracy and speed, particularly in the selection of step size, can lead to a decrease in overall performance.

3.2.2Particle Swarm Optimization (PSO)

The Particle Swarm Optimization (PSO) method is a relatively new evolutionary algorithm that has gained popularity in recent years. It was introduced by Eberhart and Kennedy as an alternative to Genetic Algorithms (GAs), taking inspiration from the social behavior of bird swarms [57].

The central concept involves the progressive development of particles to systematically navigate a range of possibilities in search of the most favorable solution. At each iteration, the algorithm assesses the effectiveness of each particle using a fitness function and adjusts its speed towards the direction of its own highest performance up to that point (referred to as P_{best}). Additionally, the algorithm identifies the best performance achieved by any particle (known as G_{best}) and incorporates this information into the velocity adjustment process [58].

During each iteration of the particle, the update formula is used to determine the velocity, position, P_{besti}, and G_{besti} for each individual particle [59]:

$$V_i^{k+1} = wV_i^k + c_1 r_1 \left(P_{besti}^k - X_i^k\right) + c_2 r_2 (G_{besti}^k - X_i^k) \qquad (3.1)$$

$$X_i^{k+1} = X_i^k + V_i^{k+1} \tag{3.2}$$

$$P_{besti} = \begin{cases} P_{besti} & f(X_i) \geq f(P_i) \\ X_i & f(X_i) < f(P_i) \end{cases} \tag{3.3}$$

$$G_{besti} = max\{f(P_{best0}); f(P_{best1}); \dots\dots; f(P_{bestm})\} \tag{3.4}$$

Where:

$$i = 1, 2, 3\ldots., \text{m}$$

m: is the number of particles, X_i and V_i are the position and velocity of particle i,k is the number of iterations. *w* is the particle inertia weight, c_1 and c_2 are learning factors, r_1 and r_2 are random numbers between (0 & 1).

The system's operational voltage is allocated to the particle's position, and the system's voltage increment is determined by the particle's speed. The greatest power point voltage obtained by each particle in the system is represented by the particle's current ideal value. The system's highest power point voltage is established as the population's optimal solution [60]. A flow chart showing the PSO algorithm is show in **Figure 3.4.**

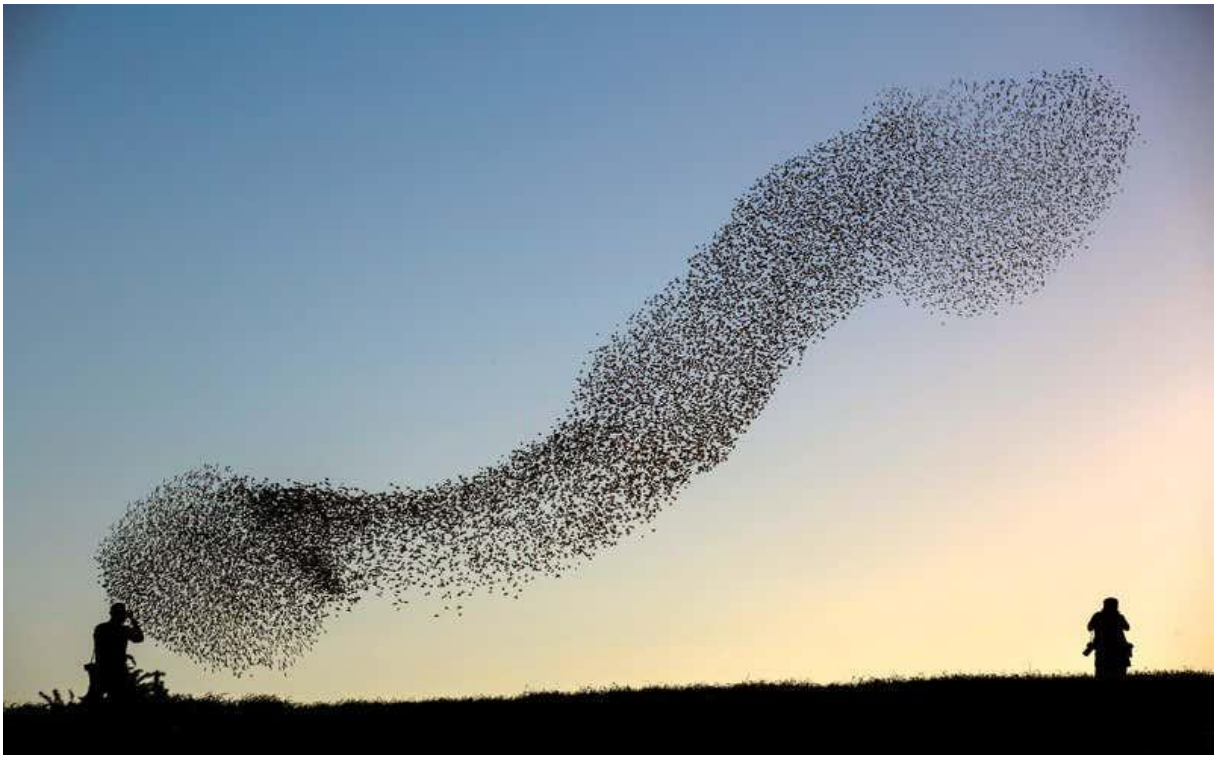

Figure 3.3 Birds swarm behavior

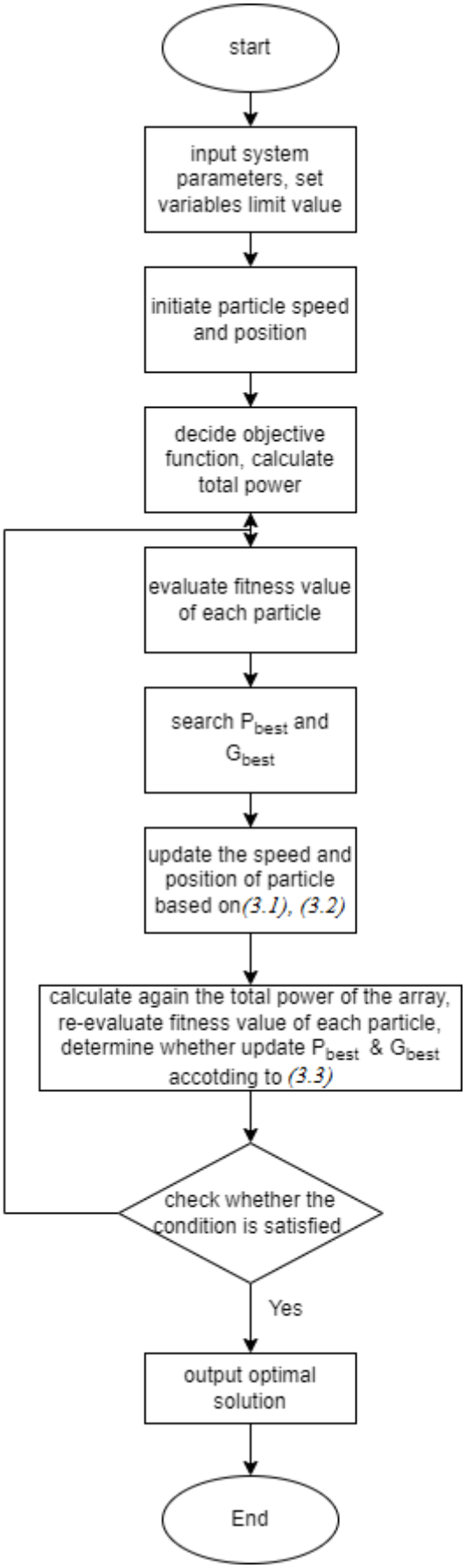

Figure 3.4 Flowchart of MPPT control based on PSO algorithm [61].

3.2.3 Grey Wolf Optimization (GWO)

The GWO algorithm is inspired by the hierarchical leadership and hunting behavior of grey wolves in nature. Grey wolves are apex predators and typically live in packs. In the GWO algorithm, four types of grey wolves, namely alpha (α), beta (β), delta (δ), and omega (ω), are used to simulate this hierarchical structure. To represent the social hierarchy mathematically, the fittest solution is designated as the alpha (α), while the second and third best solutions are referred to as beta (β) and delta (δ), respectively. The remaining candidate solutions are considered as omega (ω). **Figure 3.5** illustrates the three main steps of the GWO algorithm, which include hunting, chasing, and tracking prey. These steps are utilized to optimize the algorithm's performance. During the hunt, grey wolves encircle their prey, and this encircling behavior is mathematically modeled using the following equations [62]:

$$\vec{V} = \left|\vec{C} \cdot \vec{X}p(t) - \vec{X}p(t)\right| \quad (3.5)$$

$$\vec{X}(t+1) = \vec{X}p(t) - \vec{A} \cdot \vec{V} \quad (3.6)$$

Where *t* denotes the current iteration, ***V, A***, and ***C*** denote coefficient vectors, ***Xp*** is the position vector of the prey, and ***X*** indicates the position vector of grey wolf. The vectors ***A*** and ***C*** are calculated as follows:

$$\vec{A} = 2\vec{a} \cdot \vec{r}1 - \vec{a} \quad (3.7)$$

$$\vec{C} = 2 \cdot \vec{r}2 \quad (3.8)$$

In the GWO algorithm, a linearly decreasing component, denoted as "ɑ," ranges from 2 to 0 throughout the iterations. Additionally, "r1" and "r2" represent random vectors with values between 0 and 1. During the hunt, the grey wolves are primarily guided by the alpha, who acts as the leader, followed by the beta and delta, who also participate in hunting to some extent. The delta and omega wolves are responsible for tending to any wounded members within the pack. Therefore, the alpha is considered to possess better knowledge about the prey's location. The hunt concludes when the prey stops moving, and the grey wolves initiate an attack [62].

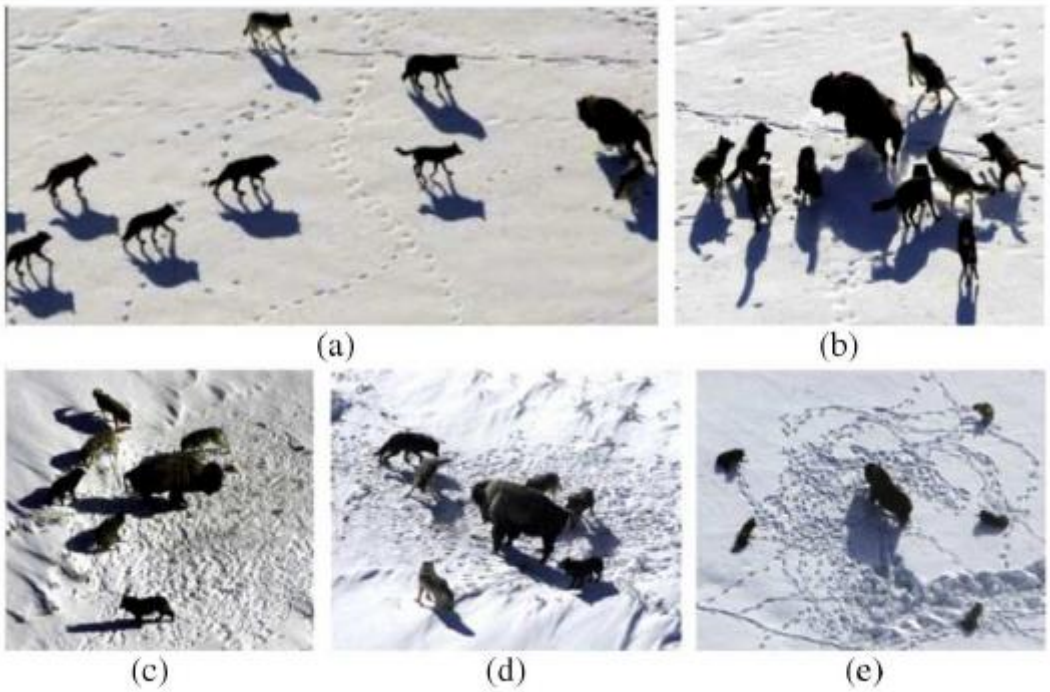

Figure 3.5 hunting behavior of grey wolves: (a)–(c) chasing and tracking prey; (d) Encircling prey; and (e) attacking prey [62].

- **Application of GWO for MPP Tracking**

The controller in the GWO-based MPPT algorithm utilizes sensors to measure V_{pv} (photovoltaic voltage) and I_{pv} (photovoltaic current) in order to determine the output power. The flowchart in **Figure 3.6** illustrates the process. In cases of partial shading, the P-V curve exhibits multiple peaks consisting of various local peaks (LPs) and one global peak (GP). When the wolves, representing the optimization agents, discover the maximum power point (MPP), their correlated coefficient vectors approach zero. The proposed method combines GWO with direct voltage control, meaning that at the MPP, the voltage is maintained at a constant value. This approach reduces the steady-state oscillations commonly found in traditional MPPT techniques, resulting in lower power loss due to oscillation and increased system efficiency. In the GWO-based MPPT implementation, the voltage V is represented as a grey wolf, leading to the modification of equation (3.5) as follows [62]:

$$V_i(k + 1) = V_i(k) - A \cdot V \qquad (3.9)$$

Thus, the fitness function of the GWO algorithm is formulated as:

$$P\left(v_i^k\right) > P\left(v_i^{k-1}\right) \qquad (3.10)$$

Where *P* represents power, *v* is the voltage, *i* is the number of current grey wolves, and *k* is the number of iterations.

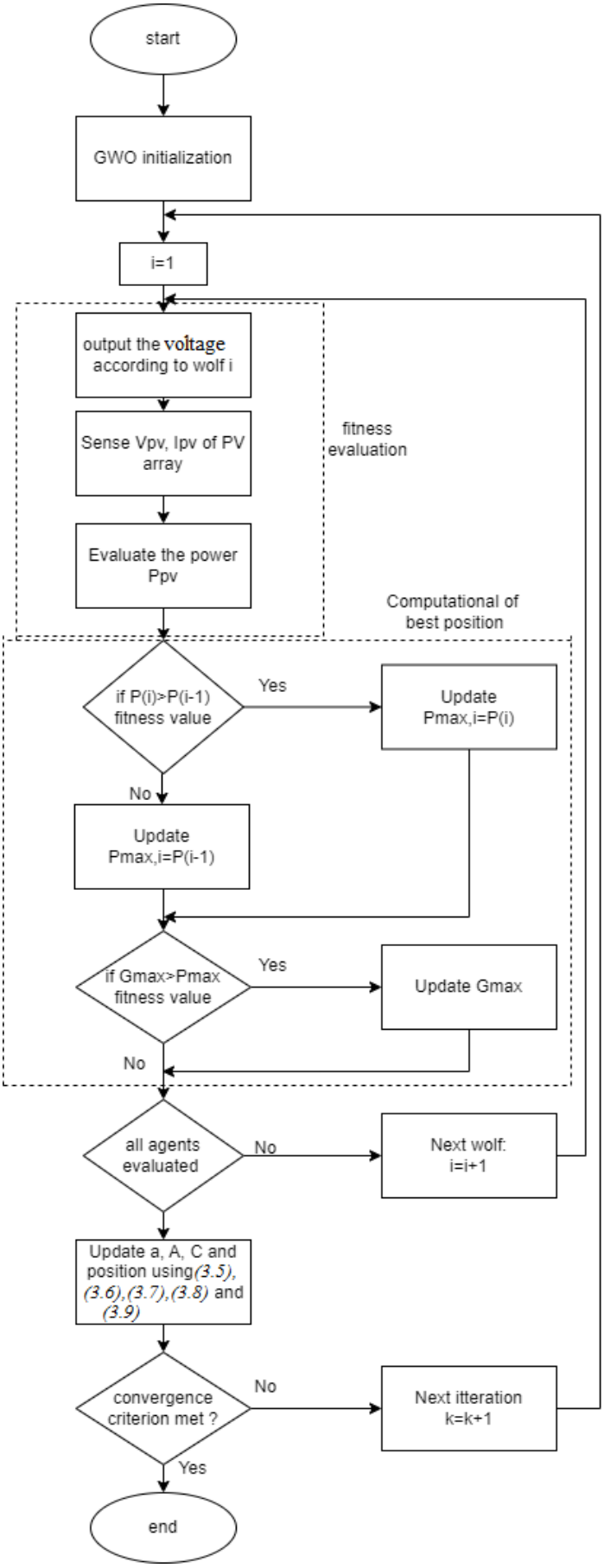

Figure 3.6 Flowchart of the proposed GWO algorithm [62].

3.2.4 Speed Reference Generation

To effectively control V_{dc} in the system, a control loop is employed. The process begins by comparing V_{ref} with V_{dc}. The resulting error is then processed through a series of stages, including a PI controller, a low pass filter, and a limiter. These phases work together to derive the desired reference value of the reference speed ω_{ref}.

Subsequently, the motor speed is regulated using PI controller, which generate the reference torque for the direct torque control. By precisely managing the motor speed, we gain control over V_{dc}. However, it's important to note that controlling V_{dc} within such a complex and interconnected loop poses significant challenges.

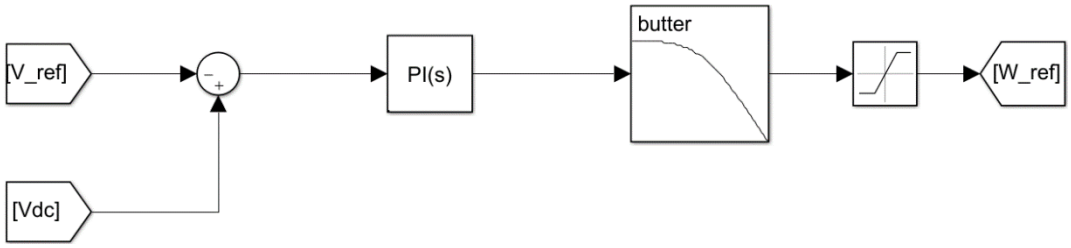

Figure 2.7 Speed reference control loop.

3.3 Direct Torque Control (DTC)

3.3.1 Basic Direct Torque Control

Takahashi introduced the concept of direct torque control (DTC) for induction motor drives in the mid-1980s. DTC involves selecting the appropriate voltage vector (switching state) for the motor's voltage inverter based on the instantaneous errors of the stator flux and electromagnetic torque. Unlike complex field orientation or current regulation loops, DTC employs separate hysteresis controllers to independently control the flux and torque. The hysteresis comparators determine the suitable voltage vector from a predefined switching table, considering the estimated position of the flux vector. Typically, a mathematical model of the induction motor is utilized to estimate the stator flux and electromagnetic torque [63].

Low and medium power applications in the industry frequently use this control strategy. The major benefits of DTC can be summed up as follows: quick drive dynamics, lack of coordinate translations and current control loops, and universal structure, where the switching table DTC can be applied to all AC machines. On the other hand, the variable switching frequency, high torque ripples, and high switching losses are the key drawbacks of DTC.

3.3.2 Principles of Direct Torque Control

Direct torque control enables independent control of the stator flux and electromagnetic torque in the fixed frame (α, β), facilitating precise and rapid response of the electromagnetic torque in induction machines. This control method utilizes a switching table to choose the suitable voltage vector. The selection of the switching states directly depends on the changes in stator flux and machine torque. Therefore, the selection is performed by constraining the magnitudes of flux and torque within two hysteresis bands. These controllers ensure separate regulation of both quantities. The hysteresis controllers take the flux and torque errors as inputs and determine the appropriate voltage vector for each commutation period [64].

3.3.2.1 Control of Stator Flux And Electromagnetic Torque

- **Control Of Stator Flux**

Basing on the IM model in stationary frame, the stator flux equation can be expressed as follows [65] [66]:

$$\frac{d_{\Psi_s}}{dt} = V_s - R_s i_s \tag{3.11}$$

and:

$$\Psi_s(t) = \int_0^{T_z} (V_s - R_s i_s) dt + \Psi_s(0) \tag{3.12}$$

$\Psi_{s(0)}$: is the flux vector at the instant *t=0s*.

When a non-zero vector is applied during the T_z sampling period, the stator resistance voltage drop $R_s i_s$ can be neglected in comparison to V_s (stator voltage) in high-speed regions. Then equation (3.12) can be written as:

$$\Psi_s(t) \approx V_s T_z + \Psi_s(0) \tag{3.13}$$

The relation between the stator voltage and the stator flux change can be established as:

$$\Delta\Psi_s = \Psi_s(t) - \Psi_s(0) = V_s T_Z \tag{3.14}$$

The Eq (3.14) means that the stator flux can be changed by the application of stator voltage during a time T_z. The stator flux vector's extremity moves in direction given by the voltage vector and making a circular trajectory **(Figure 3.8)** [67]**.**

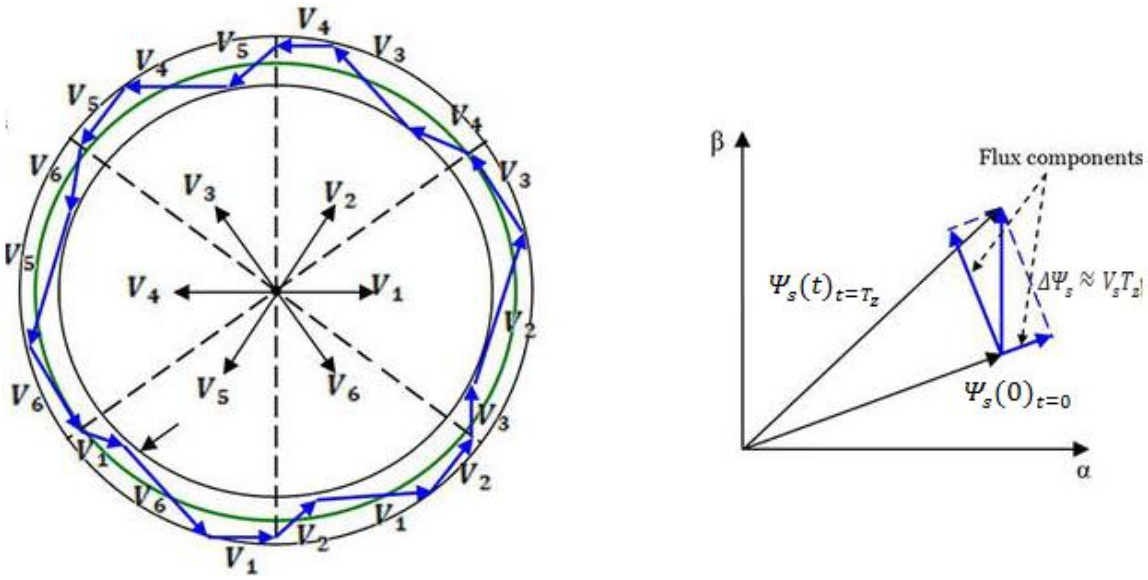

Figure 3.8 Evolution of stator flux vector in the complex plan.

The flux regulation utilizes a two-level hysteresis comparator, which enables convenient adjustment of the flux vector's outermost point. This adjustment is made within the boundaries of two closely spaced concentric circles, as illustrated in **Figure 3.9**. The selection of the hysteresis bandwidth, denoted as $h_{\Psi s}$, relies on the switching frequency of the inverter [68] [69].

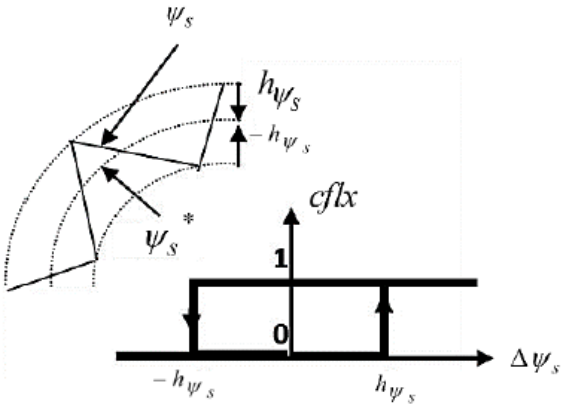

Figure 3.9 Tow-level hysteresis comparator for flux control.

The logical outputs of the flux controller are defined as:

$$\begin{cases} cflx = 1 \; if \; \Delta\Psi_s > h_{\psi s} \\ cflx = 0 \; if \; \Delta\Psi_s \leq -h_{\psi s} \end{cases} \qquad (3.15)$$

The stator flux error is defined by the difference between the references value of flux and the actual estimated value:

$$\Delta\Psi_s = |\Psi_s^*| - |\Psi_s| \quad (3.16)$$

- **Control of Electromagnetic Torque**

During one sampling period, the rotor flux vector is supposed invariant. The torque of induction motor can be expressed in terms of stator and rotor flux vectors as follows:

$$T_e = p\frac{M_{sr}}{\sigma L_s L_r}\Psi_s \times \Psi_r \quad (3.17)$$

$$|T_e| = p\frac{M_{sr}}{\sigma L_s L_r}|\Psi_s| \times |\Psi_r| sin(\delta) \quad (3.18)$$

Where:

p is the number of poles pairs.

Ψ_s, Ψ_r are stator and rotor flux vectors.

δ angle between the stator and rotor flux vectors.

If we consider equation (3.18), it becomes evident that the electromagnetic torque is influenced by the magnitudes of the stator and rotor flux. When these quantities remain constant, the torque can be managed by altering the load angle δ.

Torque regulation can be achieved by utilizing a three-level hysteresis comparator, as illustrated in **Figure 3.10**. This comparator provides control over the motor in both clockwise and counterclockwise rotation directions. On the other hand, a two-level comparator can only be used for one rotation sense.

The three-level hysteresis comparator functions by comparing the measured or estimated values of the stator and rotor flux amplitudes with predefined thresholds. These thresholds create a hysteresis band within which the flux amplitudes should ideally be maintained for desired torque regulation. If the measured or estimated flux amplitudes fall below the lower threshold of the hysteresis band, indicating insufficient torque, the comparator triggers an action to increase the load angle δ. This adjustment enhances the torque output, allowing the motor to generate more power. Conversely, if the measured or estimated flux amplitudes exceed the upper threshold of the hysteresis band, indicating excessive torque, the comparator initiates a response to decrease the load angle δ. This reduction helps in lowering the torque output, preventing any overload conditions. By continuously monitoring the flux amplitudes and dynamically adjusting the load angle based on the three-level hysteresis

comparator's feedback, precise torque regulation can be achieved. This control mechanism allows for effective management of the motor's rotational direction and ensures optimal performance in various operating conditions.

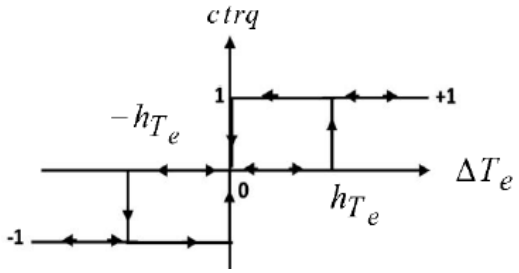

Figure 3.10 Three level hysteresis comparator for electromagnetic torque control.

The logical outputs of the torque controller are defined as:

$$\begin{cases} ctrq = 1 & if\ \ \Delta T_e > h_{Te} \\ ctrq = 0 & if\ \ h_{T_e} \leq \Delta T_e \leq h_{T_e} \\ ctrq = -1 & if\ \Delta T_e < -h_{T_e} \end{cases} \quad (3.19)$$

h_{Te} is the hysteresis band of torque.

The torque error is defined by the difference between the references values of the torque and the actual estimated values:

$$\Delta T_e = T_e^* - T_e \quad (3.20)$$

3.3.2.2 Estimation of Stator Flux and Electromagnetic Torque

- **Stator Flux Estimation**

The estimation of the stator flux is usually done by the integration of the back-emf (Electromotive force). The stator flux components can be expressed using stator voltages and currents in the stationary reference frame (α, β) by:

$$\begin{cases} \Psi_{sa} = \int_0^t (V_{sa} - R_s i_{sa}) dt \\ \Psi_{s\beta} = \int_0^t (V_{s\beta} - R_s i_{s\beta}) dt \end{cases} \quad (3.21)$$

The stator flux magnitude and flux angle can be computed as:

$$|\Psi_s| = \sqrt{\Psi_{sa}^2 + \Psi_{s\beta}^2} \quad (3.22)$$

$$\theta_s = tan^{-1}\left(\Psi_{s\beta} / \Psi_{sa}\right) \quad (3.23)$$

The stator voltage components ($V_{s\alpha}$,$V_{s\beta}$) are obtained by applying Concordia transformation on the output voltage of the three-phase VSI [70].

$$\begin{bmatrix} V_{sa} \\ V_{s\beta} \end{bmatrix} = \begin{bmatrix} 1 & -1/2 & -1/2 \\ 0 & \sqrt{3}/2 & -\sqrt{3}/2 \end{bmatrix} \begin{bmatrix} V_{sa} \\ V_{sb} \\ V_{sc} \end{bmatrix} \quad (3.24)$$

The output voltages of VSI which are the input stator voltages of the IM are given by:

$$\begin{cases} V_{sa} = \dfrac{V_{dc}}{3}(2S_a - S_b - S_c) \\ V_{sb} = \dfrac{V_{dc}}{3}(2S_b - S_c - S_a) \\ V_{sc} = \dfrac{V_{dc}}{3}(2S_c - S_a - S_b) \end{cases} \quad (3.25)$$

The stator currents components ($i_{s\alpha}$,$i_{s\beta}$) can be obtained also by applying Concordia transformation on the measured currents:

$$\begin{cases} i_{sa} = \sqrt{\dfrac{2}{3}}\, i_{sa} \\ i_{s\beta} = \dfrac{1}{\sqrt{2}}(i_{sb} - i_{sc}) \end{cases} \quad (3.26)$$

- **Electromagnetic Torque Estimation**

The electromagnetic torque generated by an induction motor can be calculated by taking the cross product of the stator variables, specifically the stator flux and stator currents. The formula to calculate the torque is expressed as follows:

$$T_e = p(\Psi_{sa} i_{s\beta} - \Psi_{s\beta} i_{sa}) \quad (3.27)$$

3.3.5 Switching Table Construction and Control Algorithm Design

3.3.5.1 Six Sectors Switching Table

To achieve independent control, a set of hysteresis comparators are utilized, which take the stator flux and torque errors as inputs. Based on the outputs of these comparators, the appropriate voltage vector is selected. However, the selection of the voltage vector is not solely determined by the hysteresis controllers' outputs; it also depends on the position of the stator flux vector. Consequently, the circular trajectory of the stator flux vector is divided into six symmetrical sectors [71].

Where: Sector 1: $^{11\pi}/_{6} \leq \theta_s < {}^{\pi}/_{6}$, sector 2: $^{\pi}/_{6} \leq \theta_s < {}^{\pi}/_{2}$, …, sector 6: $^{3\pi}/_{2} \leq \theta_s < 11\,{}^{\pi}/_{6}$

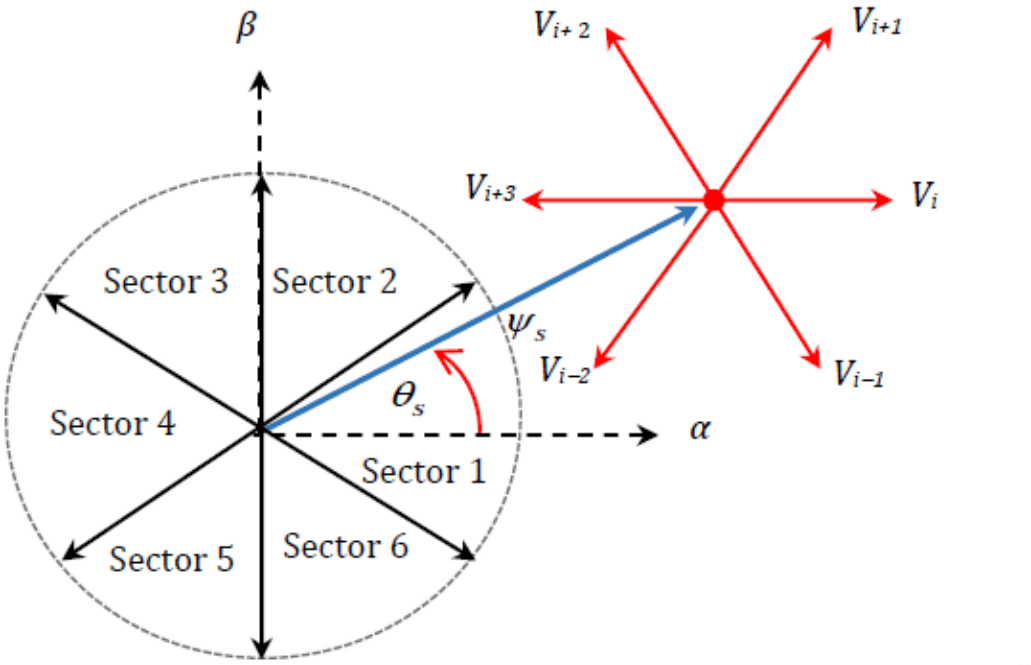

Figure 3.11 Voltage vector selection when the stator flux vector is located in sector *i* [72].

While the stator flux vector is located in the sector *i* we have [73]:

If V_{i+1} is selected, Ψ_s increases and T_e increases.

If V_{i-1} is selected, Ψ_s increases and T_e decreases.

If V_{i+2} is selected, Ψ_s decreases and T_e increases.

If V_{i-2} is selected, Ψ_s decreases and T_e decreases.

The vectors (V_i and V_{i+3}) in each sector are excluded from consideration as they can either increase or decrease the torque in the same sector, depending on the position of the flux vector in the first or second sector [74]. Selecting the zero vectors V0 and V7 will result in the stator flux coming to a halt with no change in its magnitude. Although the electromagnetic torque will decrease, it will not decrease as significantly as when the active voltage vectors are chosen [75].

Takahashi's proposed look-up table for Direct Torque Control (DTC), as presented in **Table 3.1**, Reflects these findings:

Error	Sectors	I	II	III	IV	V	VI
cflx=1	*ctrq =1*	V_2	V_3	V_4	V_5	V_6	V_1
	ctrq = 0	V_7	V_0	V_7	V_0	V_7	V_0
	ctrq = −1	V_6	V_1	V_2	V_3	V_4	V_5
cflx=0	*ctrq =1*	V_3	V_4	V_5	V_6	V_1	V_2
	ctrq = 0	V_0	V_7	V_0	V_7	V_0	V_7
	ctrq = −1	V_5	V_6	V_1	V_2	V_3	V_4

Table 3.1 Look-up table for basic direct torque control.

3.3.6 Speed Regulation In DTC Strategy

The DTC strategy involves several steps, including generating a speed reference to set the desired motor speed, and using flux and torque estimators to estimate the actual values based on measured stator voltage and current. The estimated flux, in combination with the measured data, is used to estimate the motor speed, and a speed error is calculated by comparing the estimated speed with the reference. A PI controller generates a control signal based on the speed error, which determines the voltage vector selection from the 6-sector switching table. The selected voltage vector adjusts the motor's torque and flux to minimize the speed error, and the flux and torque estimators continuously monitor the actual values to ensure accurate control. The iterative process of estimating speed, calculating error, and adjusting voltage vectors is repeated in real-time, resulting in precise speed regulation. The DTC control platform does not require the usage of a PWM inverter or a speed sensor, making it less complicated than other control methods. DTC provides accurate and fast torque dynamics and ensures high efficiency operation.

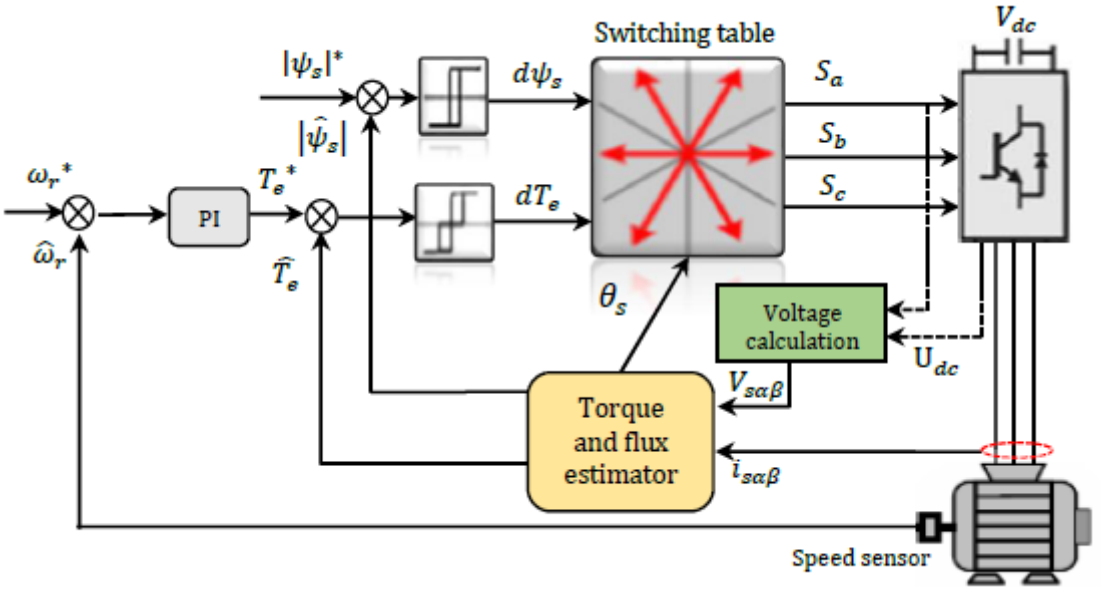

Figure 3.12 Direct torque control strategy based on lookup switching table. [76].

3.4 Conclusion

This chapter explored two key areas: maximum power point tracking (MPPT) techniques and direct torque control (DTC) strategies for induction motors. The Perturb and Observe technique was discussed as an effective MPPT algorithm for optimizing the power output of photovoltaic systems under normal operating conditions. Innovative approaches like the Grey Wolf and Particle Swarm techniques were introduced to tackle shading effects in partial shading conditions, improving the overall performance and efficiency of solar energy systems. In terms of motor control, the chapter delved into the principles and advancements of DTC, highlighting its ability to achieve precise control of stator flux and electromagnetic torque in induction motors. The Two-Level Voltage Source Inverter was emphasized as a crucial component in DTC, facilitating seamless execution of torque and flux control strategies. The chapter also provided an overview of speed control strategies in DTC, emphasizing its flexibility and adaptability for diverse industrial applications.

Chapter 4:
Simulation Results and Discussion

4.1 Introduction

This chapter will explain how the proposed stand-alone solar water pumping system's SIMULINK model was used to test and verify its functionality under various condition. The system is composed of three-phase 1.1kW 230V induction motor, connected to 1.26kW PV array with maximum voltage of 463.2V and maximum current of 2.72A tested under fixed and variable irradiance. The overall system simulation is shown in the appendix. First, we're going to test the system operation under normal condition and then under partial condition using P&O MPPT technique, Grey Wolf optimization technique and Particle Swarm optimization technique. The extra power is to recuperate the loses in the system

4.2 PV Array Characteristics

NexPower Technology NH-100UX 5A PV module will be used to simulate the PV system. The specification of the module is shown in **Figure 4.1**.

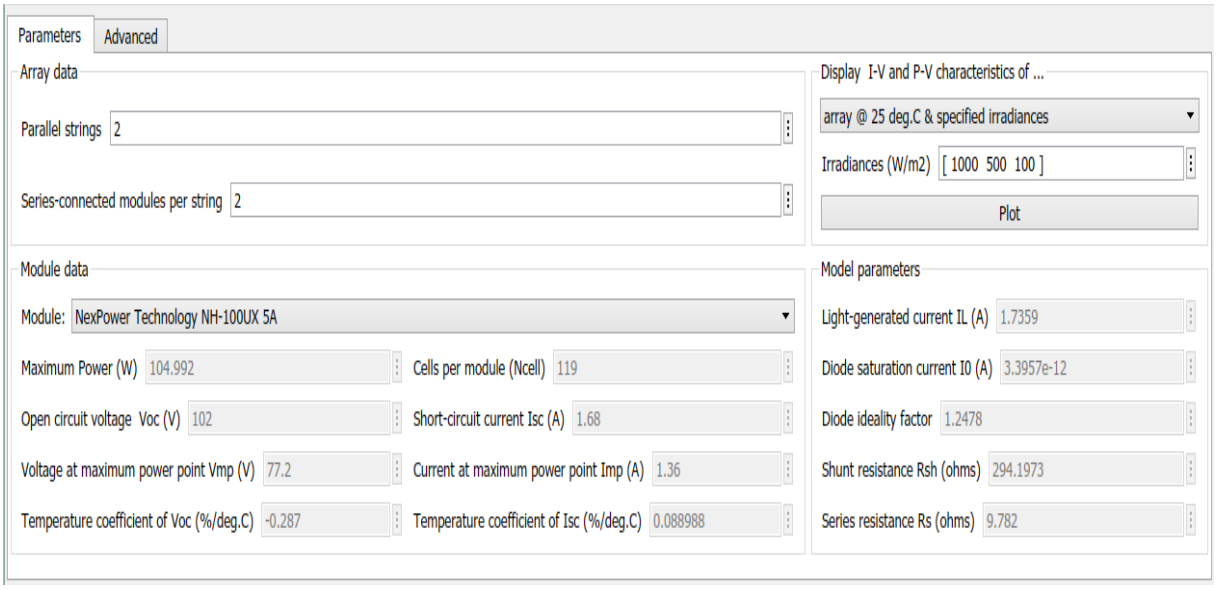

Figure 4.1 PV module specification

4.3 Simulation of The System

The water pumping system, as suggested, is simulated using MATLAB/Simulink across different scenarios involving varying irradiance levels and partial shading. The simulation outcomes for both scenarios are illustrated in the subsequent sections.

4.3.1 Under Normal Condition

The system is going to be simulated under normal condition, using P&O, GWO, and PSO MPPT algorithms. **Figure 4.3** shows the irradiance level under normal condition.

The simulation results indicate that when the solar insolation is uniform throughout, the power-voltage (P-V) curve exhibits a distinct Maximum Power Point (MPP).

Figure 4.2 shows the I-V and P-V characteristics of the PV array under normal condition and irradiance of 1000 W/m^2

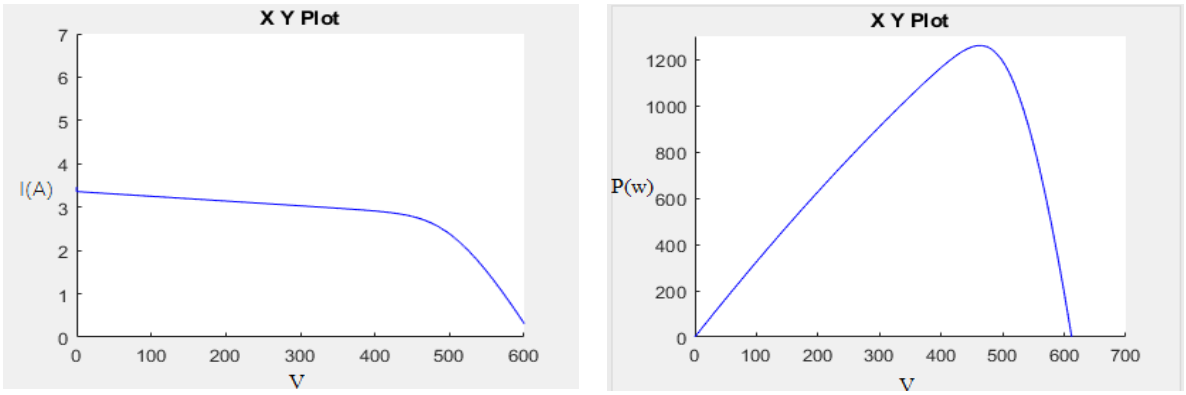

(a) (b)

Figure 4.2 a- I-V and b- P-V characteristics of three PV modules in series under uniform conditions.

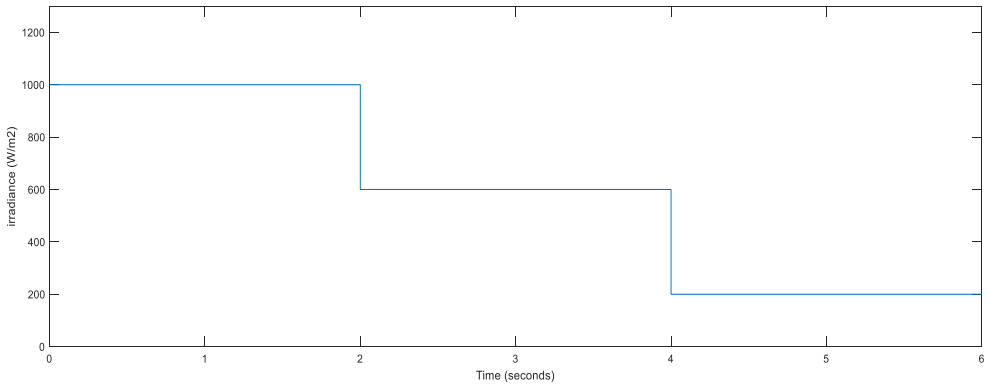

Figure 4.3 Irradiance level under normal conditions.

4.3.1.1 Solar Array Performance

The PV array performance are illustrated as follows:

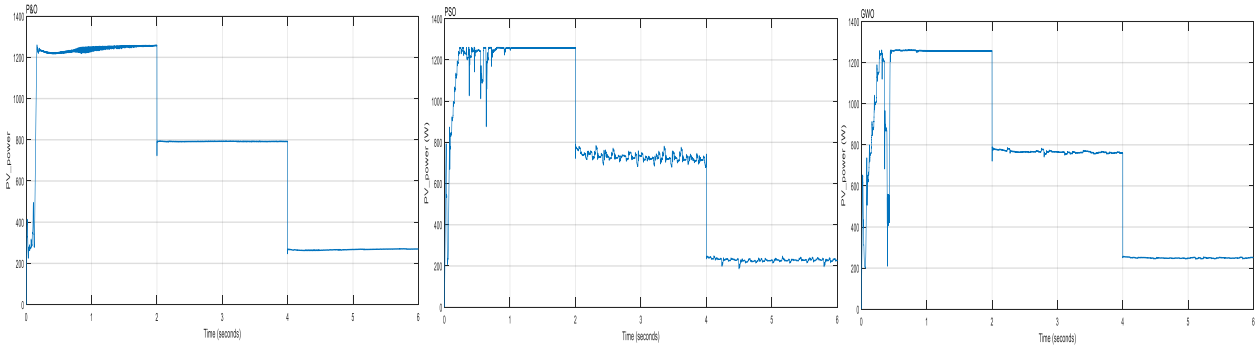

Figure 4.4 PV power under normal condition

Figure 4.4 illustrates the varying outcomes obtained from each algorithm, it can be seen that the PV power follow the irradiance profile for in case of the three algorithms. The P&O algorithm exhibits a rapid response, swiftly reaching the maximum power point (MPP). However, due to the motor's high acceleration, there is a remarkable power swing, making it challenging to maintain control over V_{dc} and prevent it from exceeding V_{best} due to motor inertia. On the other hand, the PSO algorithm produces a transient phase with more noise and requires additional time to stabilize. Even in the steady state, some residual noise persists. In contrast, the GWO algorithm delivers a slower response compared to P&O but achieves a higher level of accuracy and faster convergence compared to PSO.

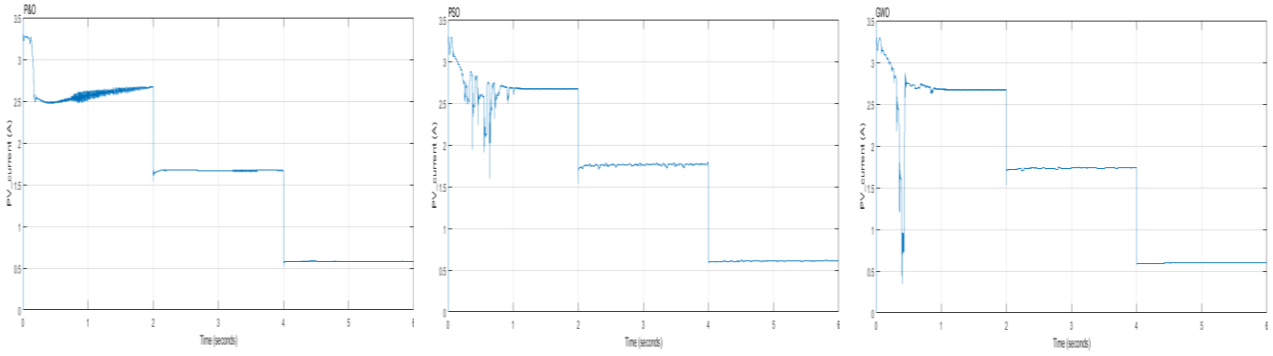

Figure 4.5 PV current under normal condition.

Figure 4.5 presents the PV current (I_{pv}), where each algorithm demonstrates unique characteristics. The P&O algorithm exhibits some noise in the steady state, which affects the stability of I_{pv}. The PSO algorithm, on the other hand, displays fluctuations during the transient state, indicating some variability in the current. In contrast, the GWO algorithm showcases a

sharp and precise response, resulting in a stable and well-controlled I_{pv} throughout the operation.

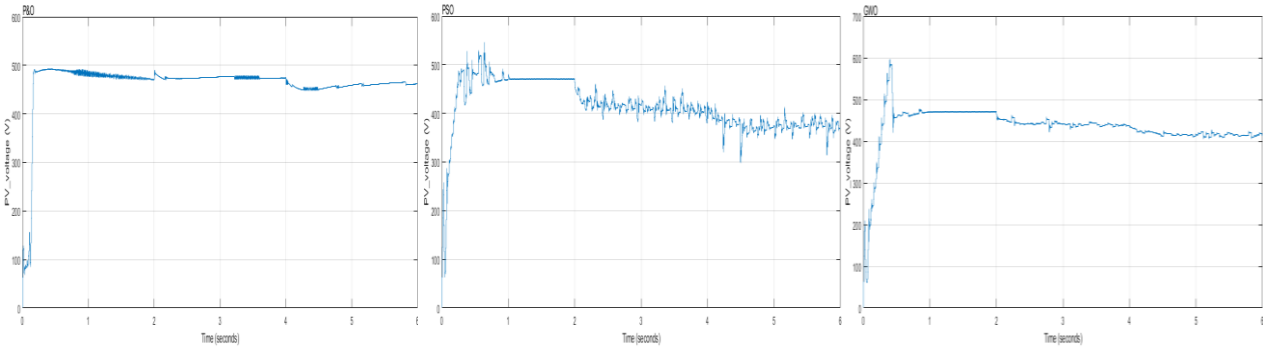

Figure 4.6 PV voltage under normal condition

In **Figure 4.6,** the PV voltage is displayed, revealing distinct responses from the algorithms. Both the P&O and GWO algorithms exhibit favorable responses with good accuracy. However, the PSO algorithm shows a noisy output, introducing more fluctuations in the PV voltage.

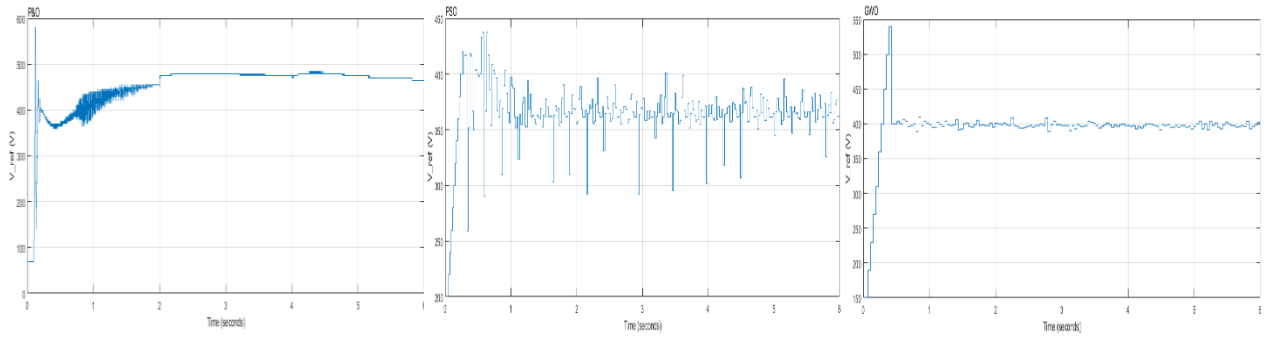

Figure 4.7 Reference voltage under normal condition

In **Figure 4.7**, the reference voltages are observed among the algorithms. The P&O algorithm exhibits a transient state with noticeable noise; however, it demonstrates a stable and reliable steady state. Conversely, the PSO algorithm tends to introduce more vibrations during operation. On the other hand, the GWO algorithm demonstrates a rapid and sharp response in the transient state, while maintaining a manageable and stable steady state.

4.3.1.2 Motor and pump performance

The motor and pump performance is illustrated as follow:

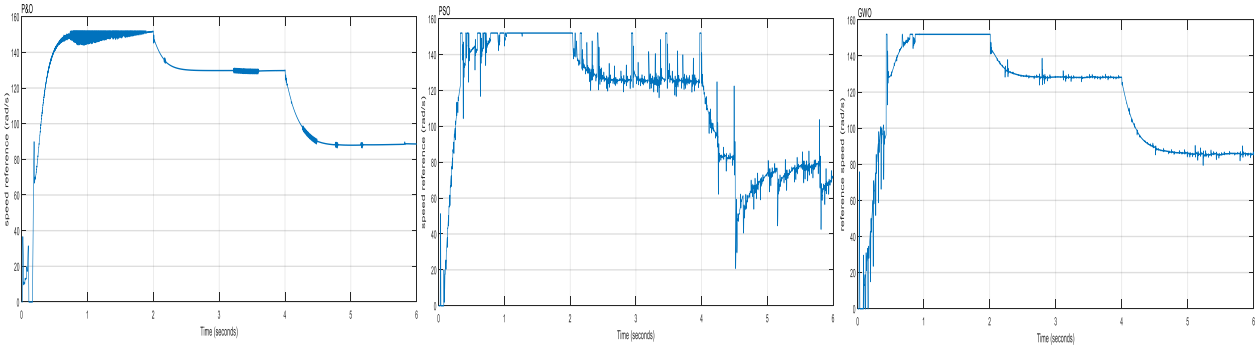

Figure 4.8 Motor speed reference under normal condition

Figure 4.8 demonstrates that the P&O algorithm exhibits noise in the steady state, while the GWO algorithm introduces noise during the transient state. The PSO algorithm lags behind in terms of performance and stability.

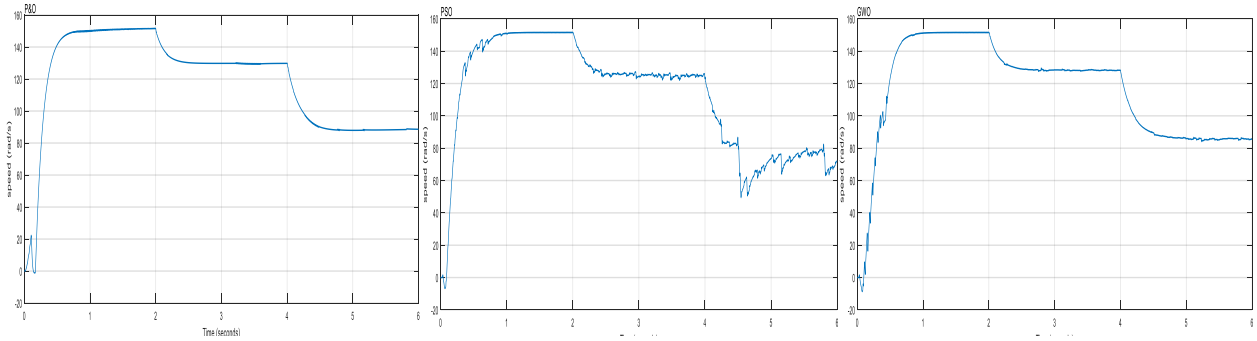

Figure 4.9 Motor speed under normal condition

As it's shown in **Figure 4.9**, demonstrates that in all cases, the motor successfully tracks the speed reference. The P&O algorithm yields the most favorable performance in terms of stability, excelling in both transient and steady states. The GWO algorithm also delivers a commendable performance, while the PSO algorithm exhibits noise and instability, particularly at lower irradiance levels.

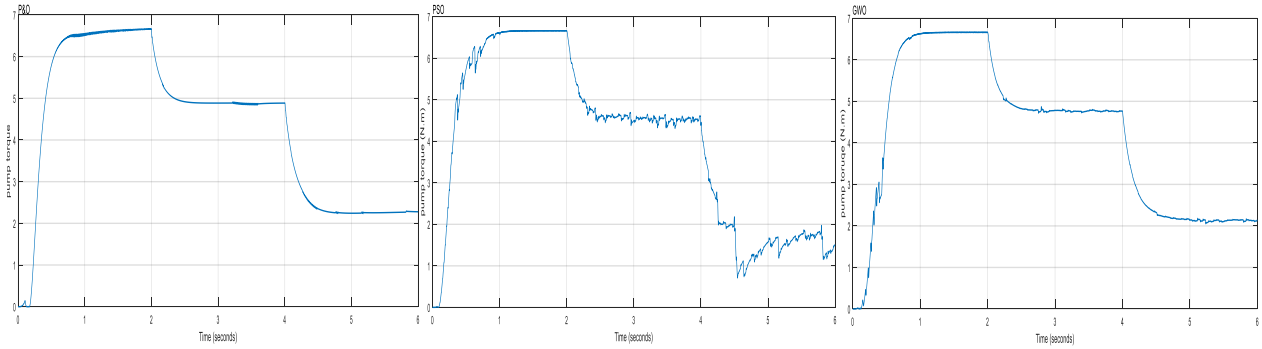

Figure 4.10 Pump's torque under normal condition.

Figure 4.10 illustrates the pump torque, since the pump torque follows the speed, the same stability and performance is shown.

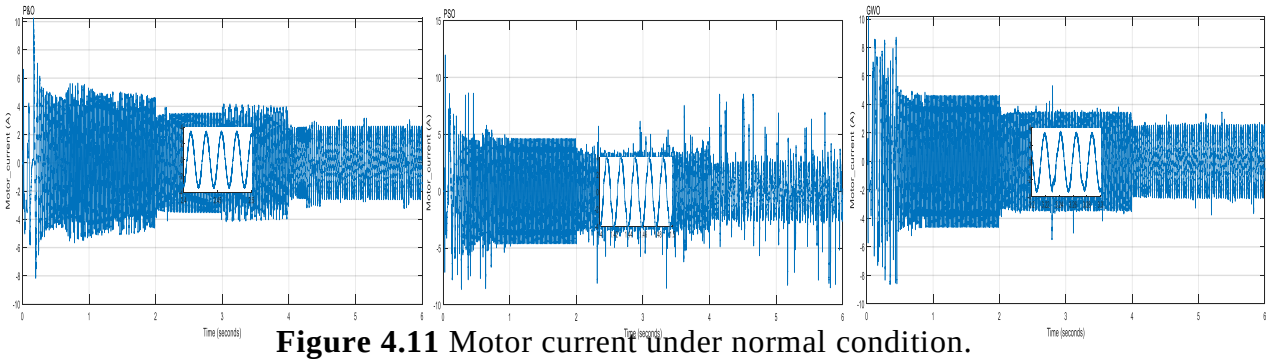

Figure 4.11 Motor current under normal condition.

Figure 4.11 illustrates the comparative behavior of the three algorithms. It is evident that both the Particle Optimization (PO) and Grey Wolf Optimization (GWO) algorithms exhibit a smooth current, whereas the Particle Swarm Optimization (PSO) algorithm demonstrates a noisier current.

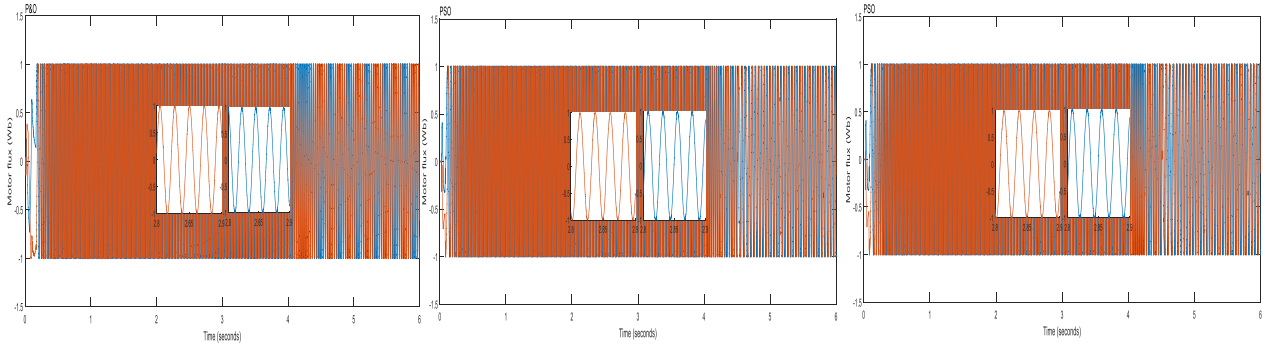

Figure 4.12 Motor flux under normal condition.

Figure 4.12 illustrates the motor flux components behavior under normal condition.

4.3.2 Under Shading Condition

In practical scenarios, the output power of a photovoltaic (PV) cell primarily depends on the solar irradiation and ambient temperature. Although the impact of ambient temperature on the PV cell is relatively small and does not directly influence the speed of dynamic response, it is essential to consider its effects. For the purpose of simulations, the working temperature of the PV cell was consistently set at 25°C. However, in real-world conditions, solar irradiance is not constant due to climate variations and the occurrence of partial shading, resulting in abrupt changes in the PV panel's output power. Consequently, it was necessary to test the algorithm across different irradiation levels to assess its ability to track and respond rapidly to these changes.

To examine the effectiveness of the perturb and observe (P&O), particle swarm optimization (PSO), and grey wolf optimization (GWO) algorithms in the presence of partial shading, three photovoltaic (PV) modules were subjected to a fixed temperature of 25°C while

being exposed to varying irradiance levels of 600, 200, and 1000 W/m^2. **Figure 4.13** shows the I-V and P-V characteristics under partial shading, we can observe the multiple peaks in the P-V curve.

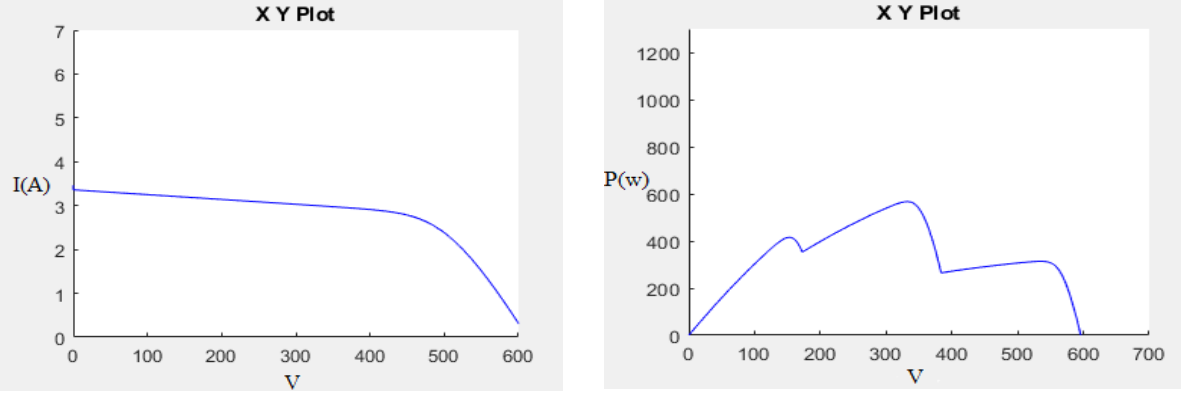

(a) (b)

Figure 4.13 a- I-V and b- P-V characteristics of three PV modules in series under partial shading condition

4.3.2.1 PV Array Performance

The PV array performance are illustrated as follows:

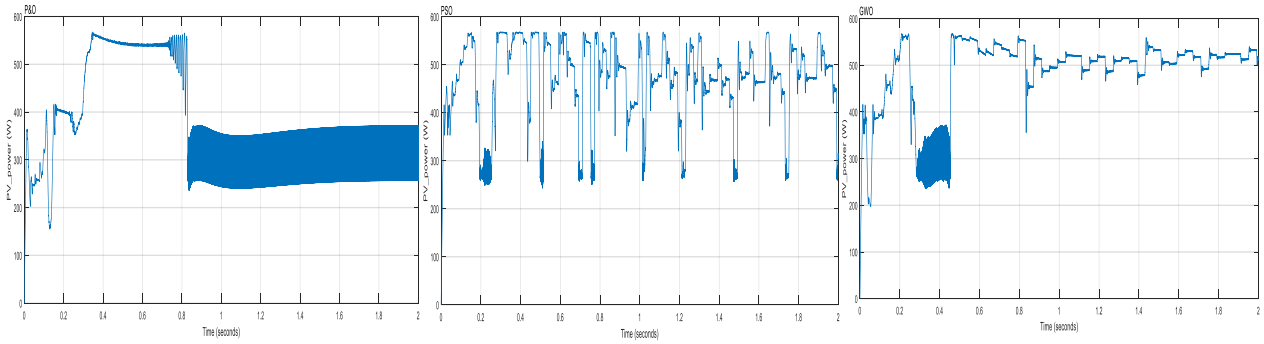

Figure 4.14 PV power under partial shading condition

Under the shade **Figure 4.14** shows, both P&O and PSO give weak performance comparing to GWO algorithm, where the last gives a higher power and a more robust performance. P&O shows inability to truck the MPP and instability. PSO can approaches the MPP but tends to take long time to stabilize.

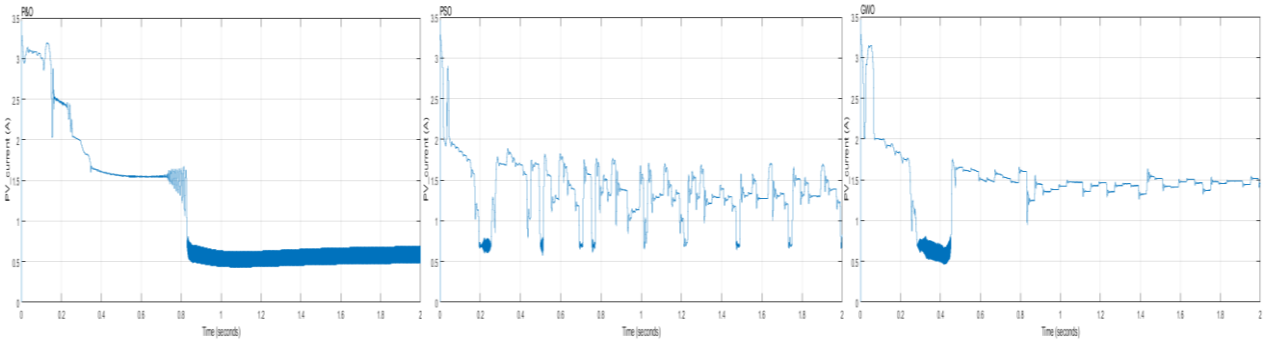

Figure 4.15 PV current under partial shading condition

Figure 4.15 depicts the PV current under shading conditions. In this scenario, the P&O algorithm exhibits less stability due to operating far from the MPP. The PSO algorithm displays fluctuations in the current, while the GWO algorithm experiences temporary instability during the transient state. However, during the steady state, the GWO algorithm delivers the best performance among the three algorithms.

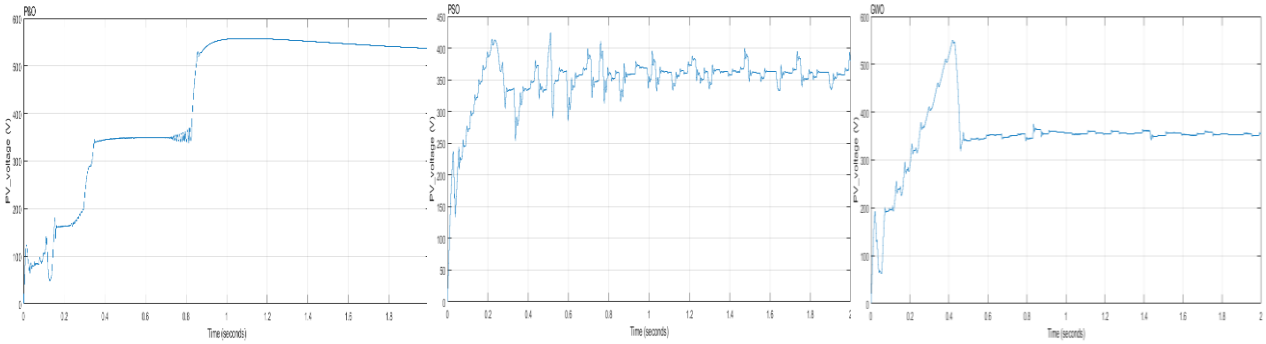

Figure 4.16 PV voltage under partial shading condition.

In Figure **4.16**, the PV voltage is shown. The P&O algorithm demonstrates a smooth response, while the PSO algorithm produces a sharp and pulsating response. The GWO algorithm also exhibits a sharp response, but with better stability

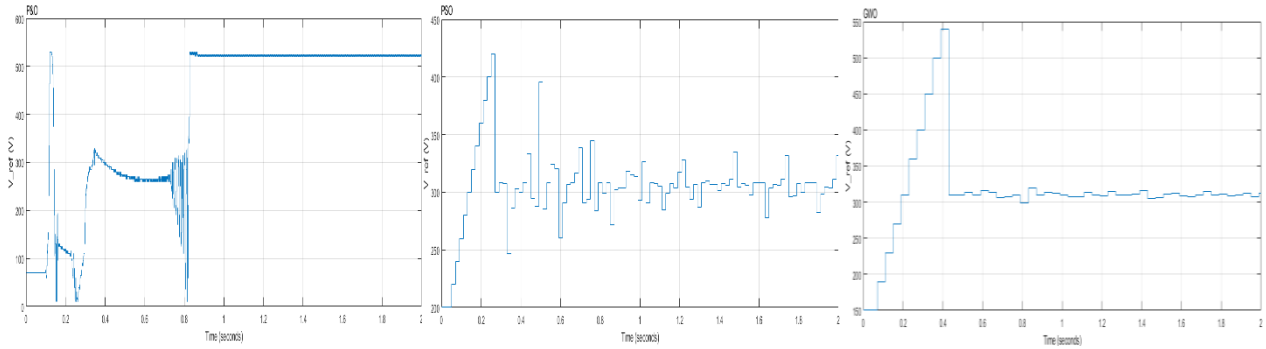

Figure 4.17 Reference voltage under partial shading condition.

Figure 4.17 displays the reference voltages under shading conditions. The P&O algorithm struggles to reach V_{best} as it attempts to track the maximum power point (MPP). Unfortunately, it gets trapped in local maxima, unable to achieve the desired voltage. The PSO algorithm approaches V_{best}, but it exhibits fluctuations around this point. In contrast, the GWO algorithm demonstrates superior tracking and stability, particularly in the steady state, outperforming the other algorithms.

4.3.2.2 Motor and Pump Performance

The motor and pump performance is illustrated as follow

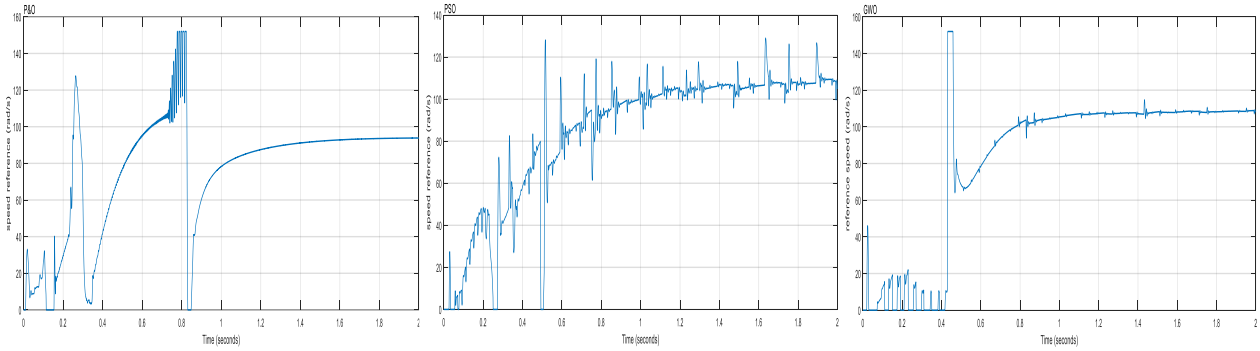

Figure 4.18 Reference speed under partial shading condition.

In **Figure 4.18**, the performance of the three algorithms is depicted, revealing distinct characteristics. The P&O algorithm exhibits swinging behavior and operates at a lower speed. The PSO algorithm introduces perturbations and pulsing, observed in both the transient and steady states. On the other hand, the GWO algorithm demonstrates fluctuations around zero speed, but it achieves higher speeds with less disturbances.

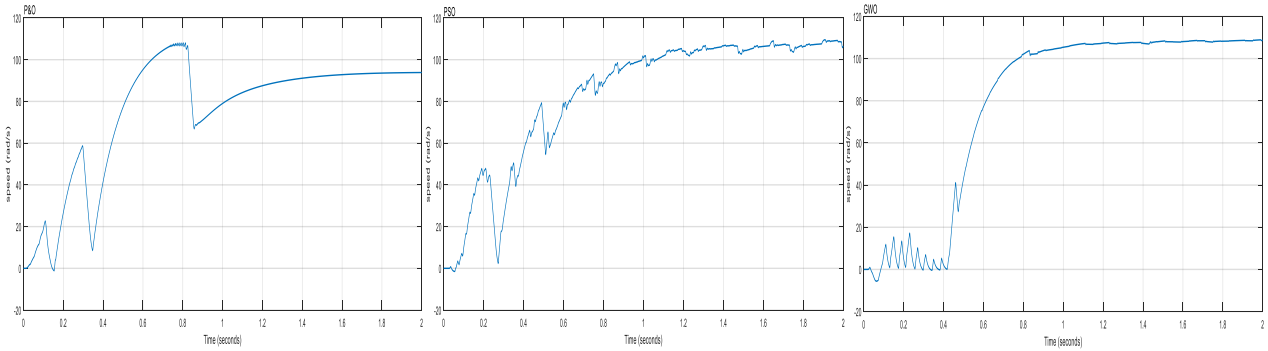

Figure 4.19 Motor speed under partial shading condition.

In **Figure 4.19**, the performance speeds of the three algorithms are displayed. The P&O algorithm demonstrates a smooth performance but at a lower speed. The PSO algorithm exhibits less stability and vibrations in the steady state. On the other hand, the GWO algorithm experiences a slower transient state and faces difficulties in starting the motor as it scans the P-V curve for G_{best}. However, once the GWO algorithm identifies the best region, it achieves higher speeds with lower vibrations, ultimately providing superior performance.

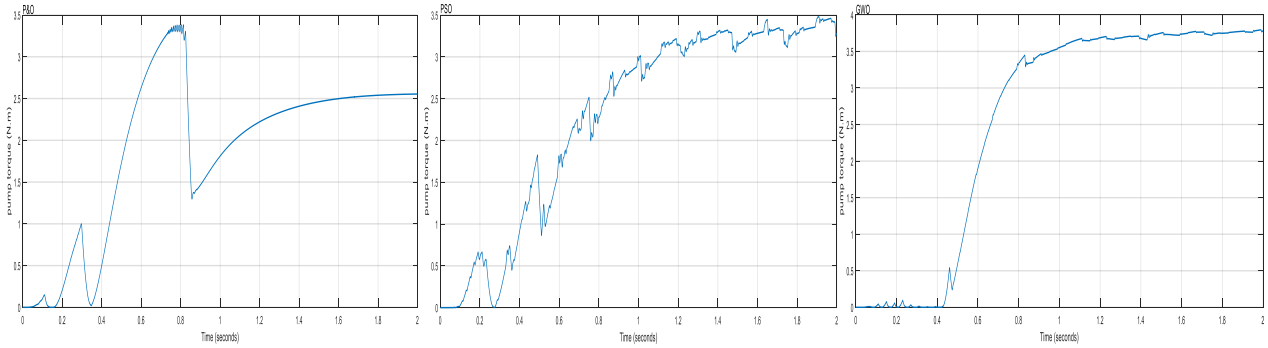

Figure 4.20 Pump torque under partial condition

Figure 4.20 shows the pump torque under partial condition. Since the pump follows the motor speed, the same performance is given.

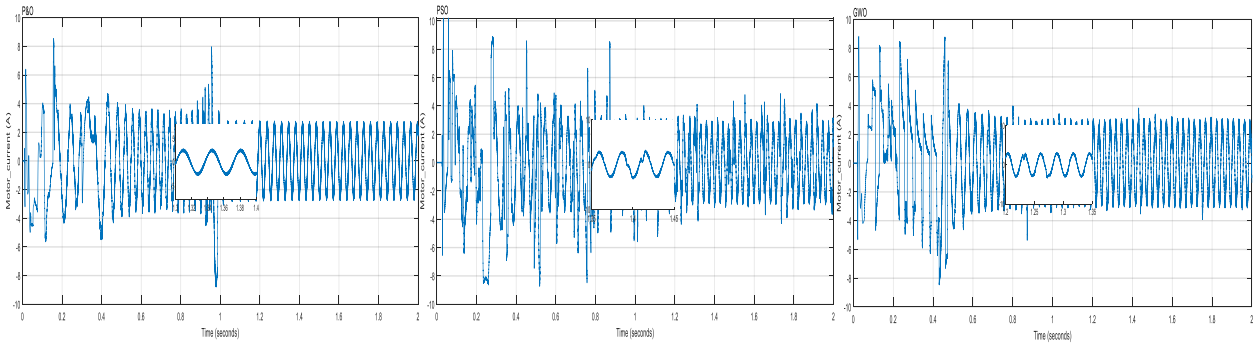

Figure 4.21 Motor current under partial condition.

In the **Figure 4.21**, it can be observed that all three algorithms exhibit noise during the transient state. However, as the algorithms converge, the Particle Swarm Optimization (PSO) and Grey Wolf Optimization (GWO) algorithms display a smoother and more stable current. On the other hand, PSO algorithm continues to exhibit some residual noise even after convergence.

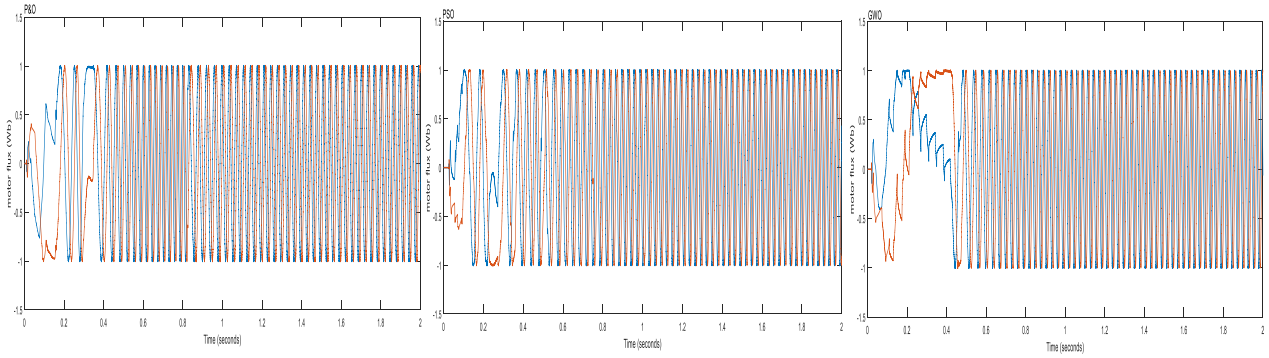

Figure 4.22 motor flux under partial shading condition.

Figure 4.22 illustrates the motor flux components behavior under partial shading condition.

In normal condition we have three values corresponding to three different level of irradiance [1000 600 200]. The maximum power that the PV array can generate according to the three irradiance levels is 1260W, 792.7W, and 270.9W respectively

The tables below show a comparison between the normal condition and partial shading condition where **Table 4.1** showing the normal results, and **Table 4.2** showing the Shading results.

Irradiance condition	**MPPT algorithm**	**Power (w)**	**Speed (rad/s)**	**Stability**			**Settling Time (s)**	
				Motor speed		**Power**	**Speed**	**Power**
Normal	**P&O**	1258 792.6 270.7	151.6 130.1 88.98	Transient Smooth	Steady state noisy	Steady state Smooth	0.7548	0.2023
	PSO	1258 732.8 231.1	151.6 126.5 82.53	Noisy	Noisy	Noisy	0.807	1.023
	GWO	1258 766.2 249.3	151.6 128.7 86.76	Noisy	smooth	Smooth	0.47	1.001

Table 4.1 comparison of the results of each MPPT algorithm showing power, speed, and settling time under noraml condition.

Irradiance condition	**MPPT algorithm**	**Power (w)**	**Speed (rad/s)**	**Stability**			**Settling Time (s)**	
				Motor speed		**Power**	**Speed**	**Power**
Shading	**P&O**	362.4	93.83	Vibration	Smooth	Unstable	1.198	1.02
	PSO	462.8	106.5	Vibration	Vibration	Unstable	1.318	>2
	GWO	524.2	108.8	Vibration	smooth	noisy	0.8367	1.8

Table 4.2 Comparison of the results of each MPPT algorithm showing power, speed, and settling time under shading conditions.

4.4 Conclusion

In conclusion, the single standalone stage solar water pumping system was simulated under both normal and partial shading conditions, utilizing three different MPPT algorithms: Grey Wolf Optimization (GWO), Particle Swarm Optimization (PSO), and Perturb and Observe (P&O), showing the performance of Solar PV array, the Induction motor, and the pump torque.

Under normal conditions, the P&O algorithm demonstrated fast response and smooth output power. However, it exhibited power swings due to challenges in controlling the voltage (V_{dc}) and preventing it from exceeding the optimal voltage (V_{best}). These difficulties were primarily attributed to motor inertia. On the other hand, the PSO algorithm took some time to converge and identify the global best (G_{best}) under normal conditions, while the GWO algorithm required a longer stabilization period.

Under partial shading conditions, the P&O algorithm showed reduced stability and limited ability to track the optimal power point (P_{best}). The PSO algorithm also faced challenges in accurately tracking the MPP due to the fluctuations caused by shading. Similarly, the GWO algorithm encountered difficulties in stabilizing and efficiently tracking the MPP under shading conditions.

Overall, the performance of the MPPT algorithms was influenced by the presence of shading. The algorithms exhibited varying levels of instability, tracking limitations, and power fluctuations under partial shading. It is important to note that the motor's performance was also impacted by the power and voltage levels, and its efficiency diminished when operating below certain thresholds.

General Conclusion

In response to a worldwide transition towards renewable energy sources, humanitarian and development organizations are progressively adopting solar photovoltaic technology for their water delivery initiatives. This shift is primarily driven by various factors, such as the affordability and dependability of solar technology.

In conclusion, this work proposed and designed a stand-alone single-stage solar water pumping system driven by an induction motor. The PV array played a central role in supplying the pump with its rated power, which was directly influenced by the varying irradiance levels (shading, normal) and ambient temperature conditions. To ensure accurate and reliable tracking of the Maximum Power Point (MPP) under changing irradiance levels, three MPPT algorithms, namely Perturb and Observe (P&O), Particle Swarm Optimization (PSO), and Grey Wolf Optimization (GWO), were employed.

The research presented in this work was divided into four chapters, each focusing on essential aspects of the system. The first chapter provided a comprehensive theoretical background on solar water pumping systems, photovoltaic theory, and their significance in the field. The second chapter focused on the modeling and design of the system, with emphasis on the PV cell and the mathematical model of the induction motor and PV array system. The third chapter delved into the control strategies, discussing the theory and flowcharts of each MPPT algorithm and the Direct Torque Control (DTC) techniques employed to regulate the motor. In the final chapter, the system was simulated using MATLAB/Simulink, evaluating the performance of each algorithm in terms of the PV array, induction motor, and pump. Comparisons were made to determine the algorithm's effectiveness under different conditions.

Through the simulations and analysis, it was observed that all three MPPT algorithms contributed to improved performance of the system by accurately tracking the MPP. However, under varying conditions, certain algorithms demonstrated superior performance. The results highlighted the adaptability of the PSO and GWO algorithms, particularly in shaded environments, while the P&O algorithm performed well under normal conditions.

Overall, this work has contributed to the understanding and development of a stand-alone single-stage solar water pumping system. The research demonstrated the importance of efficient MPPT algorithms in optimizing the system's performance and harnessing maximum power from the PV array. The findings can guide the design and implementation of more

reliable and efficient solar water pumping systems, facilitating the utilization of renewable energy for sustainable water management.

Future Work

- Experimental implementation of the proposed SWPS.
- Application of another optimization based MPPT algorithms to the system.
- Application of improved control methods for the motor such as Model Predictive Control.

Appendices

A) Motor parameters

Induction Motor parameter	value
Rated power	1100 W
Supply voltage	Three-phase, V
Stator resistance	6.75 Ω
Stator inductance	0.5192H
Rotor resistance	6.21 Ω
Rotor inductance	0.5192H
Mutual inductance	0.4957 H
Rated speed	1480.14 rpm
Vrms	230 V
frequency	50 Hz
Inertia	0.0140 kg.m²
Friction factor	0.002 N.m.s
Rated torque	7 N.m
Pole pairs	2

Table A.1 Induction Motor parameters

B) PI Speed controller

The used PI controller in the outer speed loop for all control schemes is the antiwindup controller. The dynamic equation and the transfer function using Laplace transform of the speed loop are given as following:

$$\frac{d\omega_r}{dt} = -\frac{f}{J}\omega_r + \frac{T_e}{J} - \frac{1}{J}T_L \qquad (A.1)$$

$$G_{\omega_r}(s) = \frac{\omega_r(s)}{T_e(s) - T_L(s)} = \frac{1}{Js + f}$$

The transfer function (TF) of the PI controller is defined as follow:

$$PI = K_p s + \frac{K_i}{s} \qquad (A.2)$$

Kp and *Ki* are the proportional and integral gains.

s is Laplace operator.

Then, **Figure.A.1**. Shows the block diagram of the speed control loop.

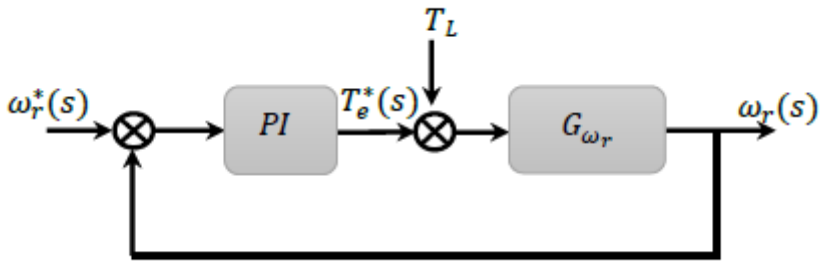

Figure A.1 Speed control loop.

By considering the load torque T_L as a disturbance. The global transfer function of the speed control in open loop becomes:

$$G_{\omega_r}(s) = \frac{\omega_r(s)}{\omega_r^*(s)} = \frac{1}{Js + f}\left(K_p s + \frac{K_1}{s}\right) \qquad (A.3)$$

In closed loop, the TF becomes

$$G_{\omega_r}(s) = \frac{K_p s + K_i}{Js^2 + (K_p + f)s + K_i} \qquad (A.4)$$

By identification member to member, the denominator of the equations (A.4) with the canonical form of second order system given in (A.5):

$$G(s) = \frac{1}{s^2 + 2\zeta\omega_n s + \omega_n^2} \qquad (A.5)$$

Where ω_n is the natural frequency and ζ is the damping coefficient. We obtain:

$$\begin{cases} \dfrac{J}{K_i} = \dfrac{1}{\omega_n^2} \\ \dfrac{K_p + f}{J} = 2\zeta\omega_n \end{cases} \qquad (A.6)$$

The gains are determined for a damping coefficient $\zeta = 1$.

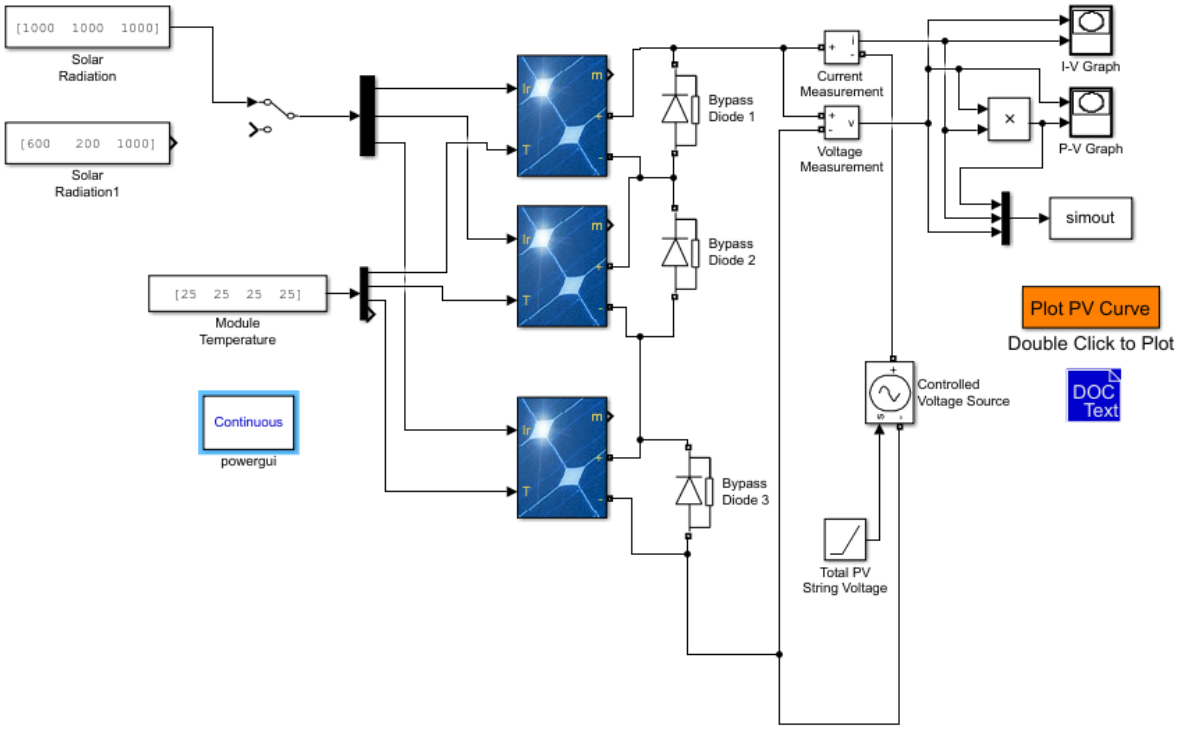

Figure A.2 SIMULINK model of five PV modules in series under uniform conditions.

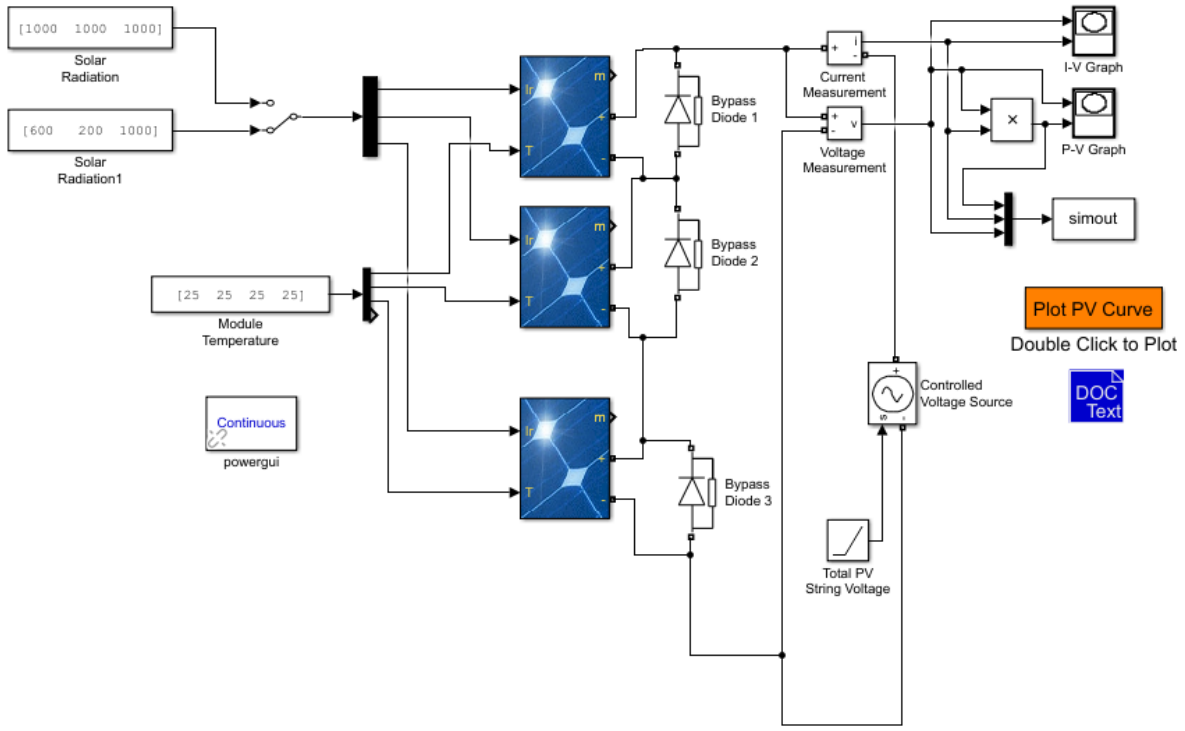

Figure A.3 SIMULINK model of five PV modules in series under partial shading conditions.

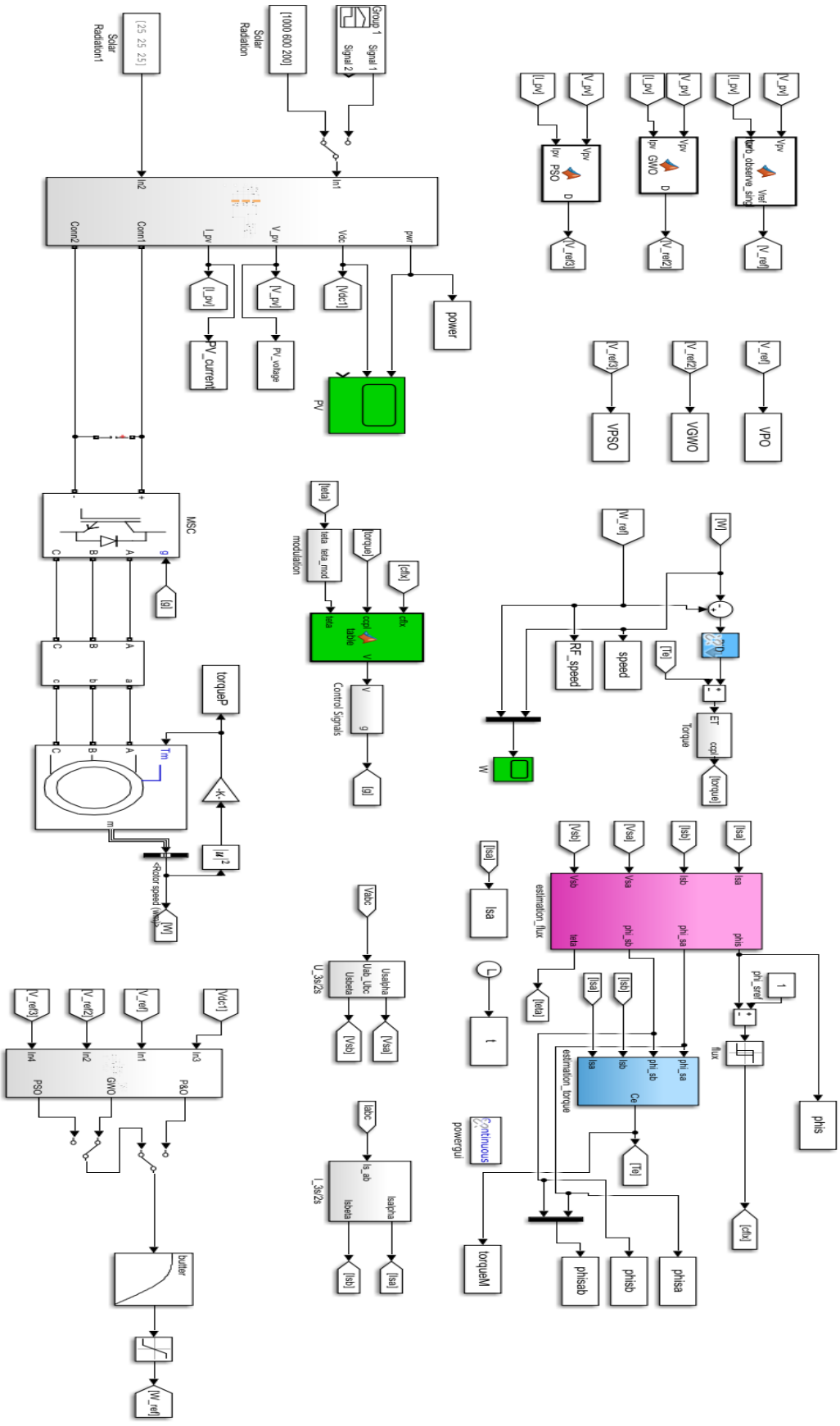

Figure A.4 The overall system's simulation

References

[1] Llario, Asenath W. Kiprono and Alberto Ibáñez, "Solar Pumping for Water Supply Harnessing solar power in humanitarian".

[2] C. Neway Argaw Denver, "Renewable Energy Water Pumping Systems Handbook," july 2004.

[3] M. Matam, V. R. Barry, and A. R. Govind, "Optimized reconfigurable PV array based photovoltaic water-pumping system," *Solar Energy,* vol. 170, p. 1063–1073, 2018.

[4] S. S. Chandel, M. N. Naik, and R. Chandel, "Review of performance studies of direct coupled photovoltaic water pumping systems and case study," *Renewable and Sustainable Energy Reviews,* vol. 76, pp. 163-175, 2017.

[5] N. Karami, N. Moubayed, and R. Outbib, "General review and classification of different MPPT techniques," *Renewable and Sustainable Energy Reviews,* vol. 68, pp. 1-18, 2017.

[6] A. Sellami, K. Kandoussi, R. El Otmani, M. Eljouad, O. Mesbahi, and A. Hajjaji, "A novel auto-scaling MPPT algorithm based on perturb and observe method for photovoltaic modules under partial shading conditions," *Applied Solar Energy,* vol. 54, no. 3, pp. 149-158, 2018.

[7] Turkenburg, Wim C., renewable energy technologies.

[8] Kalogirou, by Prof. Soteris, Solar Energy Fundamentals, Design, Modeling and Applications.

[9] Kalamkar, V. C. Sontake and V. R., "Solar photovoltaic water pumping system—A comprehensive review," *Renew. Sustain. Energy Rev,* vol. 59, pp. 1038-1067, jun 2016.

[10] Gillett, Jeff Kenna and Bill, Solar Water Pulping: A Handbook.

[11] P. Garc´ıa, C. A. Garc´ıa, L. M. Fernandez, F. Llorens, and F. Jurado, "ANFIS-based control of a grid-connected hybrid system integrating renewable energies, hydrogen and batteries," *IEEE Trans. Ind. Informa,* vol. 10, no. 2, pp. 1107-1117, May 2014.

[12] Lo Piano, Samuele, Mayumi, Kozo, "Toward an integrated assessment of the performance of photovoltaic power stations for electricity generation," 2017.

[13] Andrej Čotar, dipl.ing. REA Kvarner Ltd., Photovoltaic systems, january 2012.

[14] M. Rezkallah, A. Chandra, M. Tremblay, and H. Ibrahim, "Experimental implementation of an APC with enhanced mppt for standalone solar Photovoltaic Based Water Pumping Station".

[15] Eker, Dr Bülent, "SOLAR POWERED WATER PUMPING SYSTEMS," *Trakia Journal of Sciences,* vol. 3, no. 7, 2005.

[16] A. Khiareddine, C. Ben Salah, and M. F. Mimouni, "Strategy of energy control in PVP/battery water pumping system," *in Proc. Int. Conf. Green Energy, Sfax, Tunisia,* pp. 49-54, 2014.

[17] A. Boussaibo, M. Kamta, J. Kayem, D. Toader, S.Haragus, and A. Maghet, "Characterization of photovoltaic pumping system model without battery storage byMATLAB/Simulink," in *in Proc. 9th Int. Symp. Adv. Topics Electr.Eng.*, Bucharest, Romania, 2015.

[18] Marinescu, I. Ducar and C., "Efficiency analysis of a hydro-pump storage system for frequency support in microgrids," in *in Proc. IEEE Int. Conf. Autom., Qual. Test., Robot*, Cluj-Napoca, Romania, 2016.

References

[19] W. V. Jones, "Motor selection made easy: Choosing the right motor for centrifugal pump applications," *IEEE Ind. Appl. Mag,* vol. 19, no. 6, p. 36–45, Nov./Dec. 2013.

[20] Vimal Chand Sontake, Vilas R. Kalamkar, *solar photovoltaic water pumping system - A comprehensive review,* Nagpur,India, Department of Mechanical Engineering, St.Vincent Pallotti College of Engineering & Technology.

[21] P. Vas, Sensorless vector and direct torque control, 1998, p. 729.

[22] Ankireddy Narendra, Naik N. Venkataramana, Anup Kumar Panda, Nshit Tiwary,Amit Kumar, "A Single-Stage SPV-Fed Reduced Switching Inverter-Based Sensorless Speed Control of IM for Water Pumping Applications," *International Transactions on Electrical Energy Systems,* vol. 2022, p. 12, 2022.

[23] R. K. Bhim Singh, "Solar PV powered BLDC motor drive for water pumping using Cuk converter," *IET Electric Power Applications,* 01 February 2017.

[24] Shadab Murshid, and Bhim Singh, "Single Stage Autonomous Solar Water Pumping System Using PMSM Drive," *IEEE Transactions on Industry Applications.*

[25] M. Dubey, S. Sharma,R. Saxena, "Solar PV Stand-Alone Water Pumping System Employing PMSM Drive," in *Proc. IEEE SCEECS Conf*, Mar. 2014.

[26] H. Moussa, M. Fadel and H. Kanaan, "A single-stage DC-AC boost topology and control for solar PV systems supplying a PMSM," in *Proc REDECConf*, Nov. 2012.

[27] Chen, C. Julian, Physics of Solar Energy, 1st ed. Hoboken, NJ, USA: John Wiley & Sons Inc, 2011.

[28] "Wikimedia Commons," [Online]. Available: http://upload.wikimedia.org/wikipedia/commons/7/7d/Operation_of_a_basic_photovoltaic_cell.gif.

[29] G. Boyle, Renewable Energy: Power for a Sustainable Future, 2nd ed. Oxford, UK: Oxford University Press, 2004.

[30] Vinod a, Raj Kumar a, S.K. Singh b, "Solar photovoltaic modeling and simulation: As a renewable energy".

[31] Chaouachi, A.,Kamel,R.M., and Nagasaka,K., "A novel multi-model neuro-fuzzy-based MPPT for three-phase grid-connected photovoltaic system," *Solar Energy,* vol. 84, pp. 2219 - 2229, 2010.

[32] Mohamad Hossien Nahidan, Mehdi Niroomand, and Behzad Mirzaeian Dehkordi, "Power Enhancement under Partial Shading Condition Using a Two-Step Optimal PV Array Reconfiguration," *International Journal of Photoenergy,* no. Article ID 8811149, 2021.

[33] T. R. Seyedmahmoudian, in *Analytical Modeling of partially Shaded Photovoltaic Systems*, 2013, pp. 128-144.

[34] "Electronic Tutorials," [Online]. Available: https://www.electronics-tutorials.ws/diode/bypass-diodes.html.

[35] "PVEDUCATION," [Online]. Available: https://www.pveducation.org/pvcdrom/modules-and-arrays/bypass-diodes.

[36] "SunWize," [Online]. Available: https://www.sunwize.com/tech-notes/pv-module-bypass-diodes-what-are-they-and-what-do-they-do/.

[37] "electronics-lab.com," [Online]. Available: https://www.electronics-lab.com/article/bypass-diodes-in-solar-panels/.

[38] Mehdi Seyedmahmoudian, Saad Mekhilef, Rasoul Rahmani, "Analytical Modeling of Partially Shaded Photovoltaic Systems," vol. 6, no. 1, pp. 128-144, January 2013.

[39] Rozana Alik, Awang JusohAwang Jusoh, Tole Sutikno, "A Simple Checking Algorithm with Perturb and Observe Maximum Power Point Tracking for Partially Shaded Photovoltaic System," *TELKOMNIKA (Telecommunication Computing Electronics and Control),* vol. 14, no. 1, pp. 14-20, 2016.

[40] "SunWize, PV MODULE BYPASS DIODES-WHAT ARE THEY AND WHAT DO THEY DO?," [Online]. Available: https://www.sunwize.com/tech-notes/pv-module-bypass-diodes-what-are-they-and-what-do-they-do/.

[41] M. H. Rashid, Power Electronics: Circuits, Devices, and Applications,3rd ed. Englewood Cliffs, NJ: Prentice-Hall..

[42] Souhaib Tahir, Jie Wang, Mazhar Hussain Baloch, Ghulam Sarwar Kaloi, "Digital Control Techniques Based on Voltage Source Inverters in Renewable Energy Applications: A Review," *Electronics,* vol. 7, no. 2, p. 18, 2018.

[43] J. Rodriguez, J. Lai, and F. Peng, "Multilevel Inverters: A Survey of Topologies, Controls, and Applications," *IEEE Trans. Ind. Electron,* vol. 49, pp. 724-738, Aug. 2002.

[44] [Online]. Available: https://www.tntech.edu/engineering/pdf/cesr/ojo/parag/CHAPTER4.pdf.

[45] [Online]. Available: https://studylibfr.com/doc/10119464/chapter4.

[46] [Online]. Available: https://studylibfr.com/doc/10119464/chapter4.

[47] M. Żelechowski, *Space Vector Modulated – Direct Torque Controlled (DTC –SVM) Inverter – Fed Induction Motor Drive,* warsaw University of Technology,.

[48] IEC, "IEC 60050," in *Section 411-31: Rotation Machinery – Induction Machine – an asynchronous machine of which only one winding is energized*, october,1990.

[49] [Online]. Available: https://www.engineeringtoolbox.com/synchronous-motor-frequency-speed-d_649.html.

[50] [Online]. Available: https://home.engineering.iastate.edu/~jdm/ee554/SwingEquation.pdf.

[51] Salim Djeriou, Aissa Kheldoun, and Adel Mellit, "Efficiency Improvement in Induction Motor-Driven SolarWater Pumping System Using Golden Section Search Algorithm".

[52] Manel Hlaili, and Hfaiedh Mechergu, "Comparison of Different MPPT Algorithms with a Proposed One Using a Power Estimator for Grid Connected PV Systems," *Photovoltaic Materials and Devices,* 2016.

[53] Ajay Patel, Vikas Kumar, Yogender Kumar, "Perturb and observe maximum power point tracking for photovoltaic cell," *Innovative Systems Design and Engineering,* vol. 4, no. 6, pp. 2222-1727, 2013.

[54] Akhil Nigam, Abhishek Kumar Gupta, "Performance and simulation between conventional and improved perturb & observe MPPT algorithm for solar PV cell using MATLAB/simulink," in *International Conference on Control, Computing, Communication and Materials (ICCCCM)*, IFTM University Moradabad, UP, India, 2016.

[55] J. Ahmed, and Z. Salam, "An improved perturb and observe P&O maximum power point tracking (MPPT) algorithm for higher efficiency," *Applied Energy,* vol. 150, p. 97–108, 2015.

[56] T chaitanya, Sai Badu Ch, J Hemanth Kumar, "Modeling and Simulation of PV Array and its Performance Enhancement Using MPPT (P&O) Technique," 2011.

[57] H.Y. Shen, X.Q. Peng, J.N. Wang, and Z.K. HuA, "A multi-modality function optimization based on PSO algorithm," *ournal of Hunan University of Science & Technology,* vol. 20, pp. 78-81, sep 2005.

[58] Goçalo Calvinho, José Pombo, Silvio Mariano, Maria do Rosàrio Calado, "Design and implementation of MPPT system based on PSO algorithm," in *Internation conference of intelligent systems (IS)*, Covilha, Portugal, 2018.

[59] Ze, C., Hang, Z., Hongzhi, Y., "Research on MPPT control of PV system based on PSO algorithm," in *Chinese Control and Decision Conference*, Xuzhou, China, 2010.

[60] Wang Y, Bian N., "Research of MPPT Control Method Based on PSO Algorithm," in *Computer Science and Network Technology*, Harbin, China, 2015.

[61] Ze, C .,Hang,Z.,& Hongzhi, Y, "Research on MPPT control of PV system based on PSO algorithm," in *Chineese control and decision conference*, Xuzhou, china, 2010.

[62] Satyajit Mohanty, Bidyadhar Subudhi, Senior Member, IEEE, and Pravat Kumar Ray, Member, IEEE, "A New MPPT Design Using Grey Wolf Optimization Technique for Photovoltaic System Under Partial Shading Conditions," vol. 7, no. 1, JANUARY 2016.

[63] T. Takahashi, "A new quick-response and high-efficiency control strategy," *IEEE Trans. on Ind. Appl,* vol. 22, no. 5, pp. 820-827, 1986.

[64] Yatim, N. R. N. Idris and A. H. M., "Direct torque control of induction machines with constant switching frequency and reduced torque ripple," *IEEE Trans. Ind. Electronics.,* vol. 51, pp. 758-767, 2004.

[65] Buja GS, Kazmierkowski MP, "Direct torque control of PWM inverter-fed AC motors—A survey," *IEEE Transactions on Industrial Electronics,* vol. 51, pp. 744-757, 2004.

[66] Tiitinen P, Pohkalainen P, Lalu J, "The next generation motor control method: Direct torque control (DTC)," *European Power Electronics and Drives,* vol. 5, pp. 14-18, 1995.

[67] P. C. J.Rodríguez, Predictive control of power converters and electrical drives, John Wiley & Sons, Ltd, 2012.

[68] R. TOUFOUTI, *Contribution à la commande directe du couple de la machine asynchrone,* 2008.

[69] S. Belkacem, *Contribution à la commande directe du couple de la machine asynchrone,* 2016.

[70] M. Hafeez, M. Uddin, N. Rahim and Hew Wooi Ping, "Self-Tuned NFC and Adaptive Torque Hysteresis-Based DTC Scheme for IM Drive," *IEEE Transactions on Industry Applications,* vol. 50, no. 2, pp. 1410-1420, 2014.

[71] S. BENAICHA, *Contribution à la commande toleranteaux defauts d'un systeme a motorisation asynchrone,* 2010.

[72] Hilmi Aygun, Mustafa Aktaş, "A Novel DTC Method with Efficiency Improvement of IM for EV Applications," *Engineering, Technology and Applied Science Research,* vol. 8, no. 5, pp. 3456-3462, October 2018.

[73] Ozturk, Salih Baris, *direct torque control of permanent magnet synchronous motors with non-sinusoidal back-emf,* 2008.

[74] Pujol, Antoni Arias, *Improvements in direct torque control of induction motors,* Universitat politécnica de Catalunya, 2000.

[75] C. Zhang, L. Jia, Y. Xiao, J. He and C. Xu, "Virtual line-shafting control for permanent magnet synchronous motor systems using sliding-mode observer," *IET Control Theory & Applications,* vol. 9, no. 3, pp. 456-464, 2015.

[76] A.Ammar, ''Amélioration des Performances de la Commande Directe de Couple (DTC) de La Machine Asynchrone par des Techniques Non-Linéaires'' Ph.D thesis. 2017